JOURNAL OF GEOPHYSICAL RESEARCH, VOL. 111, D20212, doi:10.1029/2006JD007334, 2006

Assessing Goddard Institute for Space Studies ModelE aerosol climatology using satellite and ground-based measurements: A comparison study

Li Liu,[1,2] Andrew A. Lacis,[2] Barbara E. Carlson,[2] Michael I. Mishchenko,[2] and Brian Cairns[1,2]

Received 22 March 2006; revised 11 June 2006; accepted 25 July 2006; published 31 October 2006.

[1] A physically based aerosol climatology is important to address questions of global climate change. We evaluate the aerosol climatology used in the GISS ModelE (Schmidt et al., 2006), by characterizing and comparing the geographic distribution and seasonal variability of aerosol optical depth (AOD) and particle size via Ångström exponent (A) against available satellite and ground-based measurements, i.e., MODIS, MISR, POLDER, AVHRR, and AERONET data. There are a number of model parameters, particularly those related to aerosol size specification, that can be better constrained by comparison to satellite data. Our comparison shows that there are large differences in the satellite and ground-based global distributions of AOD. The differences between the observations increase for the Ångström exponent. Given the uncertainties associated with satellite retrieval results, the agreement in the distributions of global optical depth between GCM aerosols and satellite data is qualitatively reasonable. However, the Ångström exponent of the GCM aerosol is clearly biased low compared to satellite data, implying that the GCM aerosol sizes are overestimated. There is qualitative agreement of the ModelE aerosol single scattering albedo ϖ with TOMS Aerosol Index (AI) and AERONET data. The comparisons show insufficient aerosol absorption at most locations, suggesting a possible underestimation of black carbon distributions in the GCM. However, a more quantitative comparison first requires a readjustment of the GCM aerosol size specification.

Citation: Liu, L., A. A. Lacis, B. E. Carlson, M. I. Mishchenko, and B. Cairns (2006), Assessing Goddard Institute for Space Studies ModelE aerosol climatology using satellite and ground-based measurements: A comparison study, *J. Geophys. Res.*, *111*, D20212, doi:10.1029/2006JD007334.

1. Introduction

[2] Aerosols have been identified as the largest single source of uncertainty in the anthropogenic contribution to global forcing of climate change [e.g., *Charlson et al.*, 1992; *Hansen et al.*, 1997a, 1997b, 2000, 2002]. Sulfate aerosols, because of their strong negative forcing, are seen as the likely explanation for the discrepancy between modeled changes in global surface temperature and the observed temperature record [*Haywood and Boucher*, 2000]. More recently, black carbon aerosols have been identified as playing a key role in climate change, particularly in those areas that are undergoing rapid industrialization such as China and India [*Menon et al.*, 2002]. Because of the counteracting effects of absorbing and nonabsorbing aerosols, and because of large uncertainties in aerosol indirect and semidirect effects on clouds [*Intergovernmental Panel on Climate Change*, 2001], the total aerosol impact on climate is both complex and uncertain, hence there is a pressing need to study the radiative properties and the geographic and temporal variability of atmospheric aerosols.

[3] Unlike the radiative forcing of the well mixed greenhouse gases, the radiative forcing due to aerosols is more difficult to define accurately, primarily because of the large spatial and temporal variability of aerosol composition, size, mixing, and shape, all of which affect the aerosol radiative parameters and make it problematic for remote sensing measurements to characterize the aerosol radiative properties in a form that would be useful for climate modeling. Moreover, given the absence of direct observational information of global aerosol change over past decades, it becomes necessary to infer the global distribution of aerosols from chemistry transport model simulations utilizing historical trends in fossil fuel and industrial emission data. Thus validation of the GCM global aerosol climatology over the past decades can only be accomplished indirectly by comparing the GCM aerosol distributions for current climate with available satellite and ground based measurements.

[1] Department of Applied Physics and Applied Mathematics, Columbia University, New York, New York, USA.
[2] NASA Goddard Institute for Space Studies, New York, New York, USA.

0148-0227/06/2006JD007334$09.00

[4] Prior to 2002, evaluation of aerosol models was mainly carried out by comparing modeled aerosol optical depth with AVHRR retrievals over ocean and TOMS data over land, or by comparing the model results with in situ measurements like AERONET. Representative studies, to name a few, include *Chin et al.* [2002] who compared the GOCART aerosol optical depth with AVHRR and TOMS satellite data and AERONET Sun Photometer measurements, and *Penner et al.* [2002] in which AVHRR derived aerosol optical depths are compared against with 6 different aerosol models. With the launch of MODIS on board both Terra and Aqua, MISR on Terra, POLDER on ADEOS, OMI on Aura, GLAS carried on IceSat, and CALIOP on Calipso, more aerosol information has become available. *Kinne et al.* [2003] carried out a global comparison of monthly mean aerosol optical depth between models, satellite data, and AERONET ground observations. MODIS data, along with AVHRR and TOMS retrievals, were used in this study. In the paper by *Stier et al.* [2005], the composite MODIS-MISR satellite retrievals (MODIS over oceans and MISR over land) were used to assess aerosol optical depth from ECHAM5-HAM. Here, the authors compared the ECHAM5-HAM Ångström Exponent versus MODIS data to evaluate the aerosol sizes specified in the model. Field campaigns typically offer more detailed aerosol information than is available from satellite remote sensing. *Takemura et al.* [2003] analyzed not only aerosol optical depth and Ångström parameter, but also single scattering albedo, but the study was limited to the Asian Pacific area. As evident in these studies, there are large discrepancies among satellite retrievals, as well as among GCM aerosol climatologies. Reconciliation of the different data sets and achieving an understanding of the causes that are responsible for the differences, while a worthy goal, is beyond the scope of this study. After all, the scientists directly responsible for the different data sets have been working toward these goals, but have not solved all the problems. In particular, since our ModelE aerosol climatology relies on a number of best guess parameters, the objective of this study is to evaluate the GISS ModelE aerosol climatology using available satellite data and ground measurements, in order to identify potential problems in the model's treatment of aerosols and provide improved constraints for the present set of model parameters especially those related to aerosol size specification. At present, the GCM aerosols interact with the model's relative humidity fields but not with the winds or precipitation. Although GISS aerosol model has been included in other comparison studies [i.e., *Penner et al.*, 2002; *Kinne et al.*, 2003; *Yu et al.*, 2006], the aerosol climatology has never been systematically and extensively evaluated using the most recent satellite aerosol retrievals. Moreover, in contrast to the previous studies [*Kinne et al.*, 2003; *Stier et al.*, 2005], we have multiyear data sets rather than a single year of MODIS and MISR data. Multiyear averaging serves to minimize biases that may arise from a particular year. In this paper, we evaluate GISS ModelE aerosol climatology utilizing MODIS, MISR, and POLDER data supplemented by AVHRR, TOMS, AERONET measurements. The radiative parameters include the aerosol optical depth, Ångström Exponent, and single scattering albedo.

[5] The aerosol climatology used in the GISS GCM is taken from chemistry-transport model simulations which define the spatial and time dependence of the tropospheric aerosols in the form of monthly mean height-dependent aerosol mass density distributions [*Koch*, 2001]. The major species of tropospheric aerosol in the GISS ModelE GCM include sulfate, sea salt, nitrate, dust, black carbon, and organic carbon aerosols as described in sections 3.2 and 3.3 of *Schmidt et al.* [2006]. More specifically, the sulfate aerosol distributions are based on anthropogenic emission rates for SO_2 taken from the inventory of *Lefohn et al.* [1999]. A seasonally variable sea salt climatology is adapted from *Chin et al.* [2002], while nitrate aerosols are from *Liao et al.* [2004]. The industrial black carbon emissions for 1950 and 1990 are based on United Nations energy statistics as described by *Tegen et al.* [2000], and include temporal changes in fossil fuel use technologies [*Novakov et al.*, 2003]. Natural and biomass burning emissions are described by *Koch et al.* [1999] and *Koch* [2001]. Organic Carbon (OC) emissions are assumed to be a factor of 4.0 and 7.9 times those of Black Carbon (BC) for industrial and biomass, respectively [*Liousse et al.*, 1996]. Absorption by BC is increased by a factor of two to account for absorption enhancement due to internal mixing of BC with nonabsorbing aerosols [*Chylek et al.*, 1995], which in the GCM is parameterized in terms of an external mixture of aerosols. There is a further normalization, in the form of multiplicative factors of 1.9 and 2.5, respectively, that is applied to BC and OC aerosols in order to yield optimal agreement with the AERONET aerosol absorptivity [*Sato et al.*, 2003]. Mineral dust aerosols are based on aerosol transport model simulations for eight different size bins ranging from 0.1 μm to 8.0 μm effective radius [*Tegen et al.*, 1997, 2000]. For hygroscopic aerosols (sulfate, nitrate, sea salt, and OC), parametric formulas for particle growth as a function of relative humidity, including the accompanying change in density and refractive index, have been incorporated in the GISS GCM [*Schmidt et al.*, 2006].

[6] Look-up tables of Mie extinction coefficients are tabulated for relative humidities ranging from 0.0 to 0.999 separately for each aerosol type on the basis of laboratory measurements [*Tang and Munkelwitz*, 1991, 1994; *Tang*, 1996]. Laboratory measured refractive indices covering the full range of solar and thermal wavelengths [*Toon et al.*, 1976; *Nilsson*, 1979; *Volz*, 1973; *Patterson et al.*, 1977; *Kirchstetter et al.*, 2004; *Palmer and Williams*, 1974, 1975] are used to compute the Mie scattering radiative parameters for pure sulfate, nitrate, sea salt, black carbon, soil dust, organic carbon and sulfuric acid, respectively. In the ModelE aerosol climatology, the dry sizes for the different aerosol species are specified to be 0.1 μm in effective radius for back carbon, 0.2 μm for sulfate, 0.3 μm for nitrate and organic carbon, and 1.0 μm for sea salt, and eight size bins ranging from 0.1 μm to 8.0 μm for dust particles. Stratospheric aerosols (sulfuric acid) have time-variable size and optical depths [*Sato et al.*, 1993]. However, for the time period of interest, the stratospheric aerosols are at their near-zero background level. Thus the ModelE aerosol radiative parameters and their spectral dependence are based on rigorous Mie scattering results, albeit for somewhat arbitrarily specified particle sizes, hence the need for

comparison with observational data to refine the GCM aerosol parameterization.

[7] In view of the nature of the GCM aerosol data, we focus our comparisons on the monthly mean aerosol optical depth and single scattering albedo at the reference wavelength of 0.55 μm, and Ångström coefficient for the spectral interval 0.55–0.815 μm. These are the three principal radiative parameters that define the aerosol radiative forcing. The GCM aerosol climatology results presented here are computed for clear sky conditions, because remote sensing measurements of aerosols are specifically selected for cloud-free conditions. Since the GCM aerosol climatology trends are kept constant beyond 1990, the 1990 values are selected as being most appropriate for comparison with current satellite observations. Because of this, some differences between the model results and observations are to be expected because of differences in winds, clouds, and precipitation, which would affect the aerosol distribution. The principle satellite data sets used for comparison are from MODIS, MISR, POLDER, and AVHRR, with additional data from TOMS, and AERONET ground-based measurements.

[8] Aerosol optical depth (AOD, also denoted as τ) defines the atmospheric aerosol burden. Given the model-simulated atmospheric distribution and composition of aerosols, the aerosol optical depth can be calculated provided the complex refractive indices, size distributions, and hygroscopic properties of the aerosols are known. Aerosol mass loading per unit area M and optical depth are related by [*Lacis and Mishchenko*, 1995]

$$\tau = \frac{3Q_{ext}M}{4\rho r_{eff}}, \tag{1}$$

where ρ is the specific density of the aerosol, Q_{ext} is the extinction efficiency factor (at λ = 0.55 μm), r_{eff} is the effective radius (cross section weighted radius over the size distribution [*Hansen and Travis*, 1974]). The Ångström exponent (A, also denoted as α), is a measure of the effective particle size, and is typically computed over a specified spectral interval in the form of

$$A = -\ln\left(\tau_{\lambda_1}/\tau_{\lambda_2}\right)/\ln(\lambda_1/\lambda_2). \tag{2}$$

For typical tropospheric aerosols, the Ångström exponent tends to be inversely proportional to particle size with larger values of A associated with smaller aerosols. Because of the complexity of the actual aerosol size distribution, and being a mixture of different aerosol types, the Ångström exponent serves as a more reliable indicator of aerosol size than the effective radius [*Mishchenko et al.*, 1999]. The single scattering albedo ϖ has particular climatological significance since the critical single scattering albedo at which the aerosol impact on global mean surface temperature changes from cooling to heating occurs in a relatively narrow range with $\varpi_c \approx 0.86$ for climate simulations with fixed clouds, but $\varpi_c \approx 0.91$ for the case of interactive clouds [*Hansen et al.*, 1997a].

[9] In the following, we first describe the data sets used for evaluating the GISS GCM aerosol climatology (section 2). In section 3, we present results of our comparison study. This is followed by a discussion of some of the problems and limitations of the different data sets. A summary of the main results is given in section 5.

2. Aerosol Data Sets

2.1. MODIS, MISR, and POLDER Data

[10] Given that climate change is a global problem, the GCM aerosol climatology is likewise global in nature, hence satellite measurements are needed for a meaningful comparison. MODIS (Moderate Resolution Imaging Spectroradiometer) and MISR (Multiangle Imaging SpectroRadiometer) on board Terra launched in 1999, and MODIS aboard Aqua launched in 2002, currently provide the most comprehensive remote sensing of aerosols from space. POLDER (Polarization and Directionality of the Earth's Reflectance) on board ADEOS launched in 1996 is the first satellite sensor that utilizes polarimetric information to retrieve aerosol properties. Specifically, MODIS and MISR include in-flight calibration [*Kahn et al.*, 2005a; *Xiong et al.*, 2005]. MODIS-Terra (morning orbit) and MODIS-Aqua (afternoon orbit) have a viewing swath width of 2330 km and view the entire surface of the Earth every one to two days. Their detectors measure 36 spectral bands ranging in wavelength from 0.4 μm to 14.4 μm with moderate spatial resolution (250–1000 m), seven of which (nominal wavelength λ = 0.47, 0.55, 0.66, 0.87, 1.24, 1.64 and 2.13 μm) are used to characterize aerosol optical properties. MODIS's strength lies in its combination of wide spectral range, high spatial resolution, and in-flight calibration of visible and thermal IR bands. One shortcoming is the inability to distinguish aerosol size distribution, type, and particle shape with radiance measurements alone. A detailed description of the retrieval algorithm can be found in the literature [e.g., *Tanré et al.*, 1997; *Levy et al.*, 2003, 2004; *Remer et al.*, 2005]. The MODIS AOD retrievals over land have been found to be accurate to within their calculated uncertainties $\pm 0.05 \pm 0.2 \times$ AOD at wavelengths of 0.47 and 0.66 μm [*Chu et al.*, 2002], while the accuracy of MODIS AODs over ocean is within the calculated uncertainties $\pm 0.03 \pm 0.05 \times$ AOD at λ = 0.66 and 0.87 μm by comparing with colocated AERONET measurements [*Remer et al.*, 2002].

[11] The MISR instrument consists of nine pushbroom cameras that view the Earth in 9 different directions (four forward, four backward, and nadir) at four wavelengths (446, 558, 672, and 866 nm). By combining its multiple wavelength and multiple angle observations, MISR has the advantage of being able to retrieve aerosol type and discriminate spherical and nonspherical particles. However, the MISR products are probably more subject to cloud contamination, particularly thin cirrus, since there is no thermal channel for cloud screening. MISR has a 360 km wide swath, taking 9 days for complete global coverage, which means that monitoring of day-to-day aerosol variability is limited. The aerosol retrieval methodologies used with MISR data have been described by *Martonchik et al.* [1998] and *Kahn et al.* [2001]. *Kahn et al.* [2005b] have compared the MISR early postlaunch AOD retrievals over land and ocean with a 2-year measurement record of globally distributed AERONET Sun photometers. Their study indicates that overall about 2/3 of the MISR-retrieved AOD values fall within [0.05, or 20% $\times$

column AOD] of AERONET; more than a third are within [0.03, or 10% × column AOD].

[12] POLDER is a wide field of view imaging radiometer that has provided the first global systematic measurements of spectral, directionally polarized characteristics of the solar radiation reflected by the Earth/atmosphere system. It includes eight narrow-band channels, three of which have polarization capability (0.443, 0.67 and 0.865 μm). Retrieving aerosols over land is difficult because the contribution of the ground surface to the radiance reflected at the top of the atmosphere is generally much larger than that of aerosols. The polarization capabilities of POLDER open up a new opportunity to monitor aerosols over land surfaces since the polarization of most aerosol types is much larger than that of the underlying surfaces. In addition POLDER has the ability to retrieve aerosol shapes, which cannot be tackled by the MODIS type radiance only measurements, because polarization is very informative about the size, refractive index and shape of aerosols. POLDER algorithm over land uses the polarized radiances in the 0.865, 0.67 and 0.443 μm channels. Since the polarized radiance generated by dust and other coarse particles is typically small, large sized aerosols tend to be missed by the instrument given its limited spectral range from 0.443 to 0.865 μm [*Deuzé et al.*, 2000, 2001]. Therefore only the optical characteristics of the accumulation mode aerosol are derived over land. Whereas over the ocean, the inversion scheme is based on the spectral normalized radiances in addition to the polarized normalized radiances in the 865 and 670 nm channels. The total aerosol optical depth, the Ångström exponent, as well as the accumulation mode optical depth are deduced. Thus, over land POLDER optical depths and Ångström exponents are used for qualitative regional variability information only, and not on an equal footing comparison of total aerosols such as MODIS, MISR, AVHRR and the GCM. For illustrative purposes, we include the POLDER retrievals over land along with those over the ocean, but the readers should keep in mind that the POLDER retrieved aerosol properties over land are mainly contributed by fine mode aerosol, leading to smaller optical depth and higher Ångström exponent.

2.2. AVHRR and TOMS Data

[13] Before the launch of MODIS and MISR, remote sensing of aerosol optical properties from space was accomplished using satellite data that were not explicitly designed for this application, e.g., AVHRR and TOMS data. With a more than 2-decade record, the global two-channel Advanced Very High Resolution Radiometer (AVHRR) aerosol retrievals generated under Global Aerosol Climatology Project (GACP) provide valuable information on potential long-term trends in the spatial and temporal variability of atmospheric aerosols over the ocean. The principal limitations of this aerosol product are the limited spectral sampling, imperfect cloud screening and calibration uncertainties [*Mishchenko et al.*, 1999]. There is no point-by-point validation of the GACP AOD retrievals with in situ measurements because of the limited number of cloud-free AVHRR pixels, 4 × 4 km resolution sampled to 30 km, contained in the gridded ISCCP DX data set [*Rossow and Schiffer*, 1999]. Nevertheless, statistical comparisons with ship-borne Sun photometer results have shown good agreement. It is found that the ensemble averaged satellite-retrieved AVHRR optical depth overestimates the ensemble averaged Sun photometer data only by about 11% with a random error of about 0.04 [*Liu et al.*, 2004].

[14] The Total Ozone Mapping Spectrometer (TOMS) on board the Nimbus-7 and later on the Earth Probe satellite also provides a long-term nearly global climatology of aerosol optical depth and aerosol index (AI, which provides a measure of aerosol absorptivity) over both land and water surfaces from 1979 to present. TOMS measurements [*Torres et al.*, 1998], which sample the UV backscatter between 340 and 380 nm relative to the Rayleigh scattering background, are an important source of information on the global distribution of absorbing aerosols, in particular, windblown mineral dust and biomass burning smoke aerosols. However, the retrieved quantities are sensitive to the height above the ground of the absorbing aerosol layer and must rely on correctly prescribed aerosol types. Subpixel cloud contamination is another major issue affecting the retrieval accuracy because of the large footprint of the instrument.

2.3. Ground-Based Measurements

[15] AERONET is a globally dispersed network of nearly 400 automated ground-based sun/sky scanning radiometers which provides correlative ground-based measurements for satellite and model validation studies at specific geographic locations [*Holben et al.*, 1998; *Dubovik et al.*, 2002]. Typically, the optical depth uncertainty of AERONET measurements is about ±0.01 to ±0.02, with spectrally dependent larger errors (±0.02) in the UV spectral range [*Holben et al.*, 1998; *Eck et al.*, 1999]. The accuracy of AERONET retrieved single scattering albedo is estimated to be within 0.03 [*Dubovik et al.*, 2000]. Because of their relatively high accuracy, AERONET data are widely utilized to validate satellite retrievals and model results. The principal limitation is that with only 400 stations unevenly distributed across the globe, the measurements may not be sufficiently dense for global coverage. Table 1 presents a summary of the data sets we used to evaluate the GISS ModelE aerosol climatology.

3. Intercomparison Results

3.1. Aerosol Optical Depth and Ångström Exponent

3.1.1. Global Scale

[16] Comparison of the GISS ModelE aerosol climatology with available satellite data and AERONET measurements shows that the global optical depth distribution of GCM aerosols qualitatively agrees with satellite observations and ground-based measurements (Figures 1a and 1b). The atmospheric burden of aerosols is seen to be generally higher in summer (JJA) than in winter (DJF). The model appears to reproduce the prominent features of spatial and seasonal variations of satellite observed aerosol optical depth, such as wind blown dust over northern Africa and the Persian Gulf region, and smoke over southern Africa and South America. The aerosol loading is decidedly higher over land and near coastal regions. Aerosol optical depth is seen to decline with distance

Table 1. Description of the Data Sets We Used to Compare Against the ModelE Aerosol Climatology[a]

	MODIS	MISR	POLDER	AVHRR	TOMS	AERONET
PI and/or responsible scientists	Y. Kaufman, L. Remer	R. Kahn, J. Martonchik	F. Bréon, J. Deuzé	M. Mishchenko, I. Geogdzhayev	O. Torres	B. Holben, O. Dubovik
Some representative references	*Tanré et al.* [1997], *Remer et al.* [2005]	*Martonchik et al.* [1998], *Kahn et al.* [2001]	*Deuzé et al.* [2000, 2001]	*Mishchenko et al.* [1999], *Geogdzhayev et al.* [2002]	*Torres et al.* [1998]	*Holben et al.* [1998], *Dubovik et al.* [2002]
Aerosol parameters	AOD and A	AOD	AOD and A	AOD and A	AI	AOD, A, and ϖ
Data version	collection 004 level 3 quality assured monthly $1 \times 1^\circ$ grid averages	MISR level 3 monthly mean $0.5 \times 0.5^\circ$ data	version 03.03 over land and 04.03 over ocean, POLDER 2 (2nd generation retrieval algorithm) POLDER1 (1st generation algorithm)	most updated version	version 8	version 2 level 2 monthly mean AOD and A and version 1 level 2 and level 1.5 monthly mean almucantar retrieved ϖ
URL	http://daac.gsfc.nasa.gov	http://eosweb.larc.nasa.gov/PRODOCS/misr/level3/download_data.html	http://smsc.cnes.fr/POLDER/A_produits_scie.htm	http://gacp.giss.nasa.gov	http://toms.gsfc.nasa.gov/aerosols/aerosols_v8.html	http://aeronet.gsfc.nasa.gov
Time range of the data set used in the study	Mar 2000 to Oct 2005 for Terra and Jul 2002 to Oct 2005 for Aqua	Mar 2000 to Sep 2005	Nov 1996 to Jun 1997 for POLDER1 and Apr to Oct 2003 for POLDER2	Aug 1981 to Dec 2004 excluding the periods affected by Mt. El Chichon and Pinatubo eruptions	Jan and Jul 1990	range varies for each station
Wavelength pair for A	0.47–0.66 μm over land; 0.55–0.865 μm over ocean	NA	0.55–0.865 μm over both land and ocean	precalculated look up table between 0.65 and 0.7 μm	NA	0.47–0.87 μm

[a]AOD represents aerosol optical depth. All AODs are reported at or converted to 0.55 μm. A stands for Ångström Exponent. MISR level 3 data are stage 2 validated and contain mix versions of retrievals. However, there is no visible discrepancy, at least on large scale, between different versions of the data. MISR level 3 Ångström Exponent data are not currently available because the parameter has not been validated (R. Kahn, personal communication, 2006). POLDER data are kindly provided by Francois-Marie Bréon and are made available to us at $4 \times 5^\circ$ GCM resolution. AERONET data are converted to the $4 \times 5^\circ$ GCM grid resolution for comparison with the modeled aerosol climatology. If there is only one data point in a GCM grid box, we assumed the AERONET measurements at that location to be representative over the whole grid box. If there is more than one AERONET site in a GCM grid box, the data are combined with equal weight. NOAA AVHRR data [*Stowe et al.*, 1997] are not included because of lack of aerosol size information.

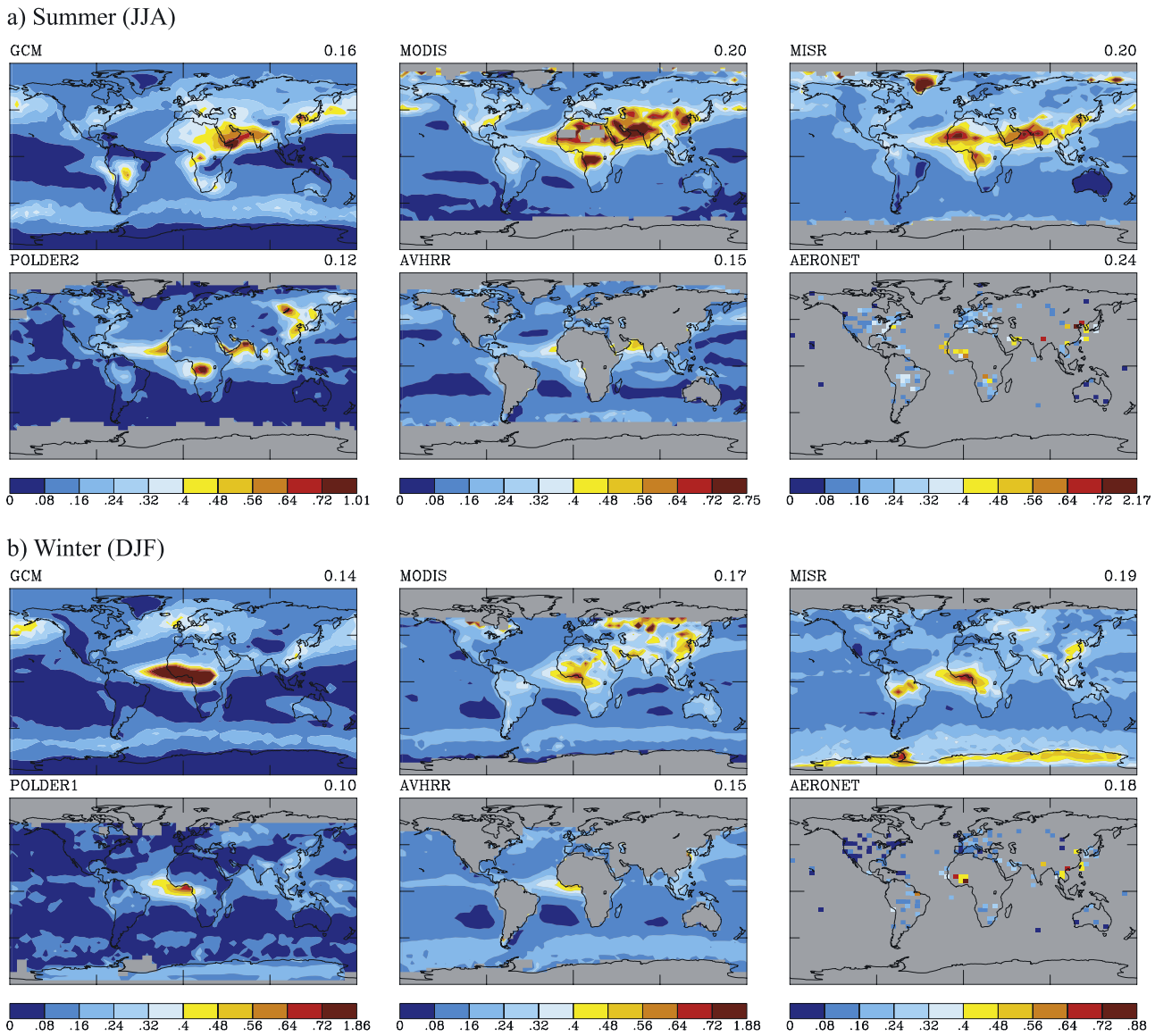

Figure 1. Qualitative agreement for the overall seasonal means of aerosol optical depth at 0.55 μm compiled from different data sets: (a) summer and (b) winter. Numbers at top right corner represent the area weighted global means with missing data skipped. The color bars are evenly scaled, except the right end numbers, which represent the maximum value for each column.

away from the continental sources, consistent with the mechanisms of aerosol transport by large-scale wind systems and deposition. Overall, air is cleaner over the open ocean and in the Southern Hemisphere. High aerosol concentrations, most likely spurious, are reported by both MODIS and MISR at high northern latitudes in JJA and by MISR at coast of Antarctica in DJF. These may arise from the difficulties in cloud screening over snow and ice surfaces. The optical depth values of POLDER are unequivocally lower than any of the other data sets even over ocean where total AOD is retrieved. Over land such trend is expected, where aerosol optical characteristics are derived for the accumulation mode only. Taking into consideration of the fact that there are no AVHRR retrievals available over land, the global mean aerosol optical depth for AVHRR is very close to that obtained by MODIS and MISR, although large regional discrepancies may exist between the data sets. For example, the AVHRR retrievals tend to produce smaller optical depths in areas with high aerosol loading. Globally the GCM aerosol optical depth climatology appears to be underestimated relative to the satellite data, but the corresponding regional patterns of AOD distribution are much more variable. The model does not have enough dust transported off the west coast of Africa. Although biased low compared to satellite observations, the GCM aerosol optical depth is in closer agreement with AERONET measurements over the central Pacific in all season and the U.S. continent in DJF. The exceptionally high aerosol concentrations produced by the GISS GCM over Sahel region in the winter season, and to a lesser extent, in the Amazon during the summer, along with the inadequate aerosol mount in South America in DJF, suggest that shortcomings in biomass burning simulations in the chemistry transport model are responsible. All data

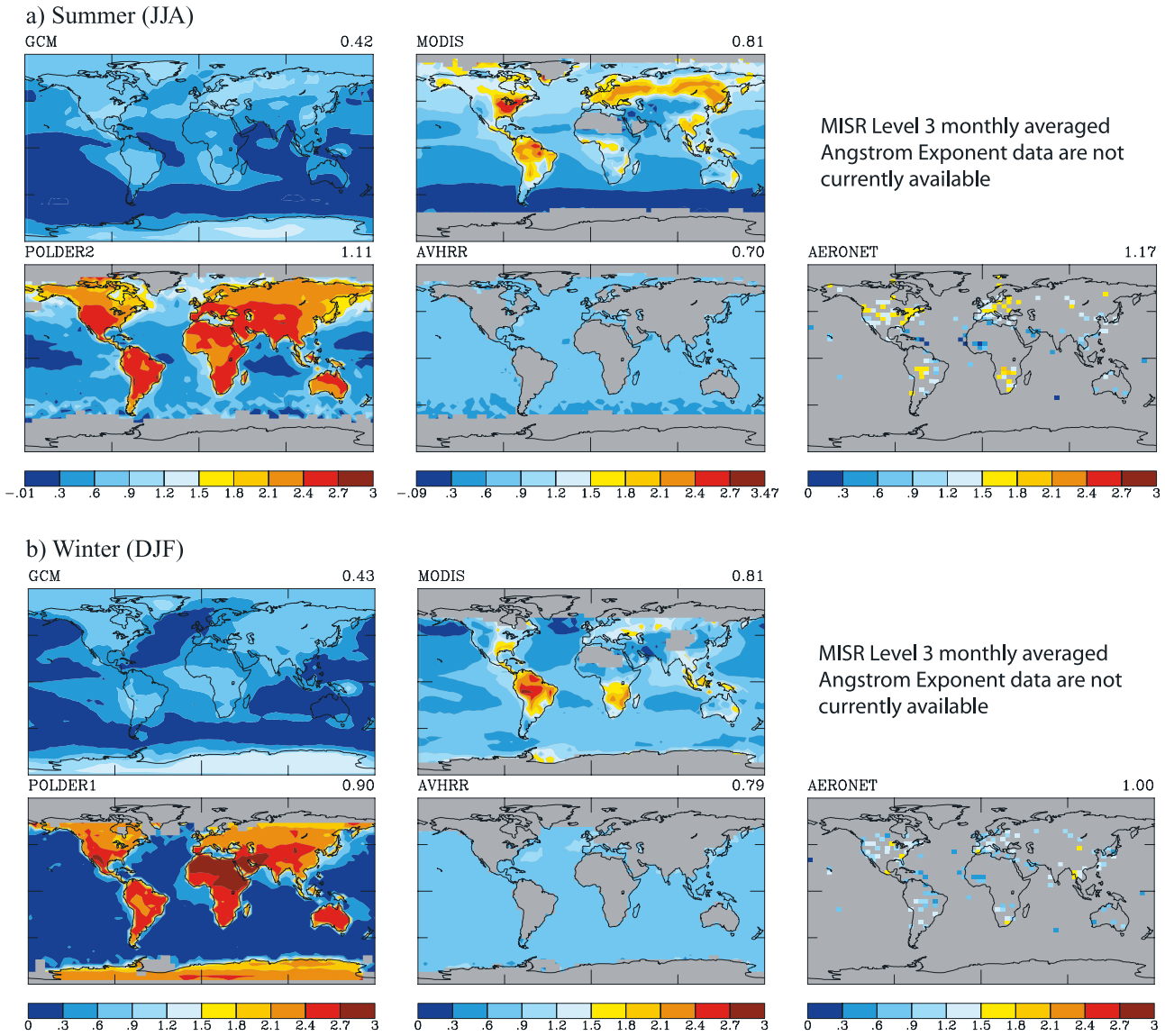

Figure 2. GCM underestimate of the overall seasonal means of Ångström exponent obtained from the whole data record for different data sets: (a) summer and (b) winter. Numbers at top right corner represent the area weighted global means with missing data skipped. The color bars are evenly scaled, except the left and right end numbers, which represent the minimum and maximum value for each column.

products show elevated aerosol optical depth in North Pacific Ocean. This might be real because of the dust, pollutant, and biomass smoke from east Asia. An interesting finding is that the GCM gets even higher AOD value near Alaska than the upstream source region during the winter, which could be related to seasonal changes in sea salt concentrations.

[17] In contrast, large spatial and temporal differences, are seen to exist for the Ångström exponent between the different data sets (Figures 2a and 2b). This may not be surprising since the Ångström exponent is obtained as the logarithmic derivative of the aerosol optical depths between two wavelengths (equation (2)), so that a small error in retrieved AOD at one or the other wavelength can be magnified into a larger error of the calculated Ångström exponent. Thus the retrieval accuracy of A is particularly problematic in clean atmospheres where the aerosol signal is small and the derivation of Ångström exponent becomes very sensitive to instrument calibration [*Ignatov et al.*, 1998; *Remer et al.*, 2005]. In addition, not all the satellite derived Ångström parameters are calculated between the same pair of wavelengths (see Table 1). While the retrieval accuracy of aerosol optical depth is well documented [e.g., *Remer et al.*, 2005; *Kahn et al.*, 2005b], there is no systematic validation for the Ångström Exponent. Nevertheless, all of the data sets tend to show a higher Ångström exponent over the land and near coastal areas, with the value decreasing toward mid-ocean, characteristic of a transition from smaller anthropogenically influenced continental particulates to generally larger oceanic sea salt aerosols. Because of the rather narrow range of the AVHRR retrieved Ångström parameter, the above described pattern is less applicable for the AVHRR data. The POLDER retrieved Ångström exponents over land tend to be much higher because the remote sensing

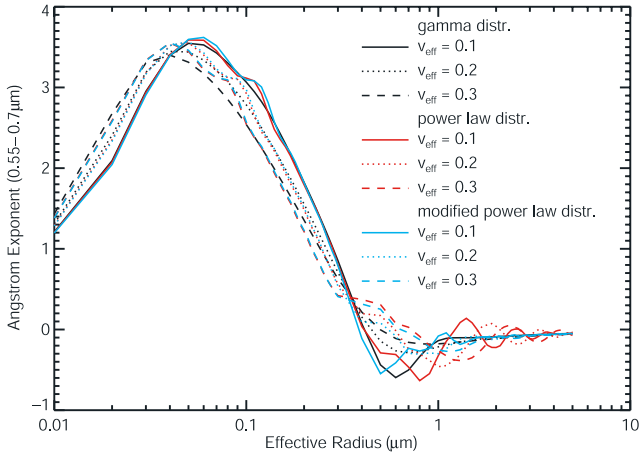

Figure 3. Ångström exponent dependence on aerosol size, computed for nominal refractive index of 1.5 + 0.003*i*, for spectral interval 0.55 to 0.7 μm versus effective radius for different size distributions.

technique utilizing the polarization signature of scattered solar radiance is more sensitive to particles within the accumulation mode. As shown in Figure 2, MODIS retrieved aerosol sizes are smaller in the eastern part of the US (as represented by large Ångström parameter) than in the west, particularly during the summer. The same pattern is also seen in the AERONET ground measurements, although to a lesser degree. Possibly this may be indicative of a greater concentration of sulfate fine mode aerosol in the east compared to the west, but further studies are needed to understand this interesting feature. The geographical distribution of Ångström exponent of the GISS GCM aerosol climatology broadly agrees with the MODIS data, but is systematically biased low in magnitude. Assuming accurate parameterization of particle growth for hygroscopic aerosols due to water absorption, we suspect that the aerosol dry sizes in the GISS GCM aerosol climatology are set too large; and this may also explain in part why the GCM aerosol optical depths are low compared to satellite observations.

[18] Given the refractive index, the Ångström exponent, or slope of spectral extinction, provides a direct measure of the aerosol size in terms of its effective radius at least for the accumulation range of interest for tropospheric aerosols. As shown in Figure 3., for absorbing aerosols (refractive index of 1.5 + 0.003*i*) that are smaller than 0.05 μm effect radius, the Ångström exponent is seen to decrease with decreasing sizes. For nonabsorbing aerosols, the Ångström exponent would increase monotonically to the Rayleigh value of A = 4, as the effective radius approaches zero. Cursory inspection of the global distribution of Ångström exponent in Figure 2 and the Ångström exponent dependence on size shown in Figure 3, suggests that the averaged effective radius of the GCM aerosol appears to be of order 0.3−0.4 μm, while the observational data suggest the value of 0.2−0.3 μm. Thus, in order to make the model results agree more with the satellite retrievals, it is desirable to reduce the averaged effective radius.

[19] Figures 4 and 5 show a surprisingly large difference in the seasonal variability of the area weighted overall monthly mean aerosol optical depth (Figure 4) and Ångström exponent (Figure 5) among the different data sets. Because of the greater variability in retrieved optical

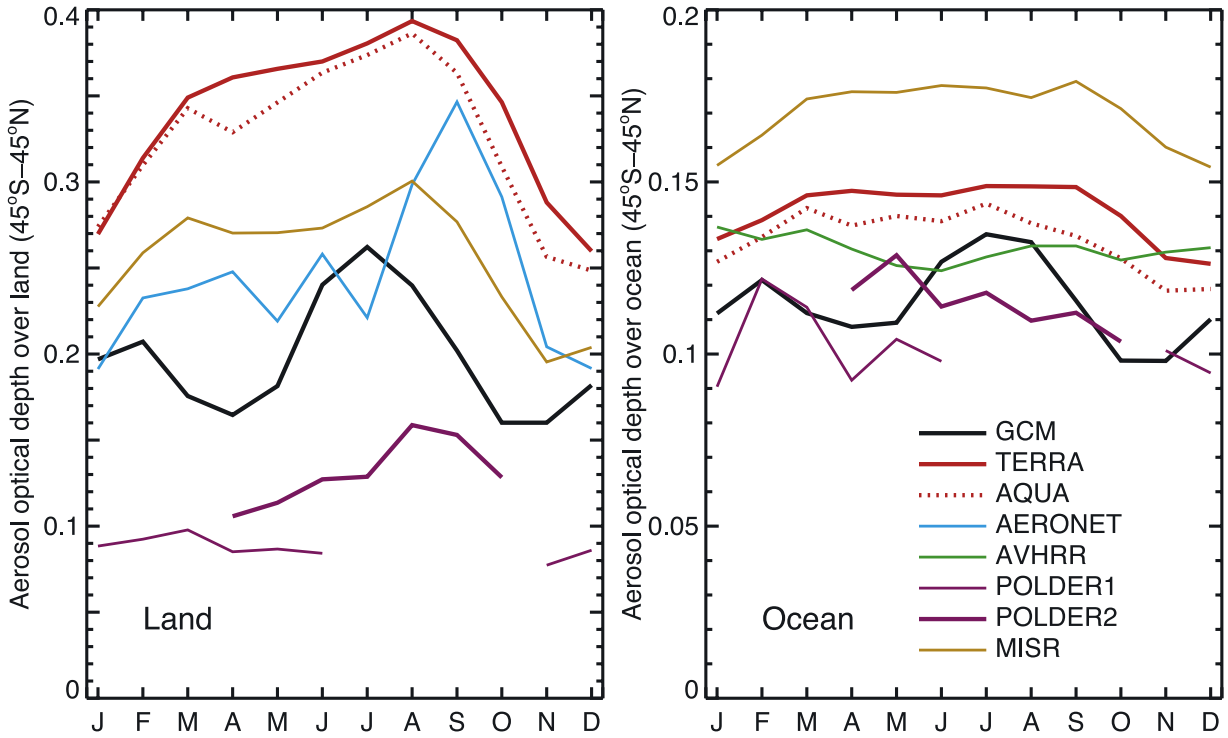

Figure 4. Seasonal dependence of area weighted overall monthly mean aerosol optical depth from different data sources. Data (left) over land and (right) over ocean have been averaged over 45°S−45°N and over available data of the respective instruments.

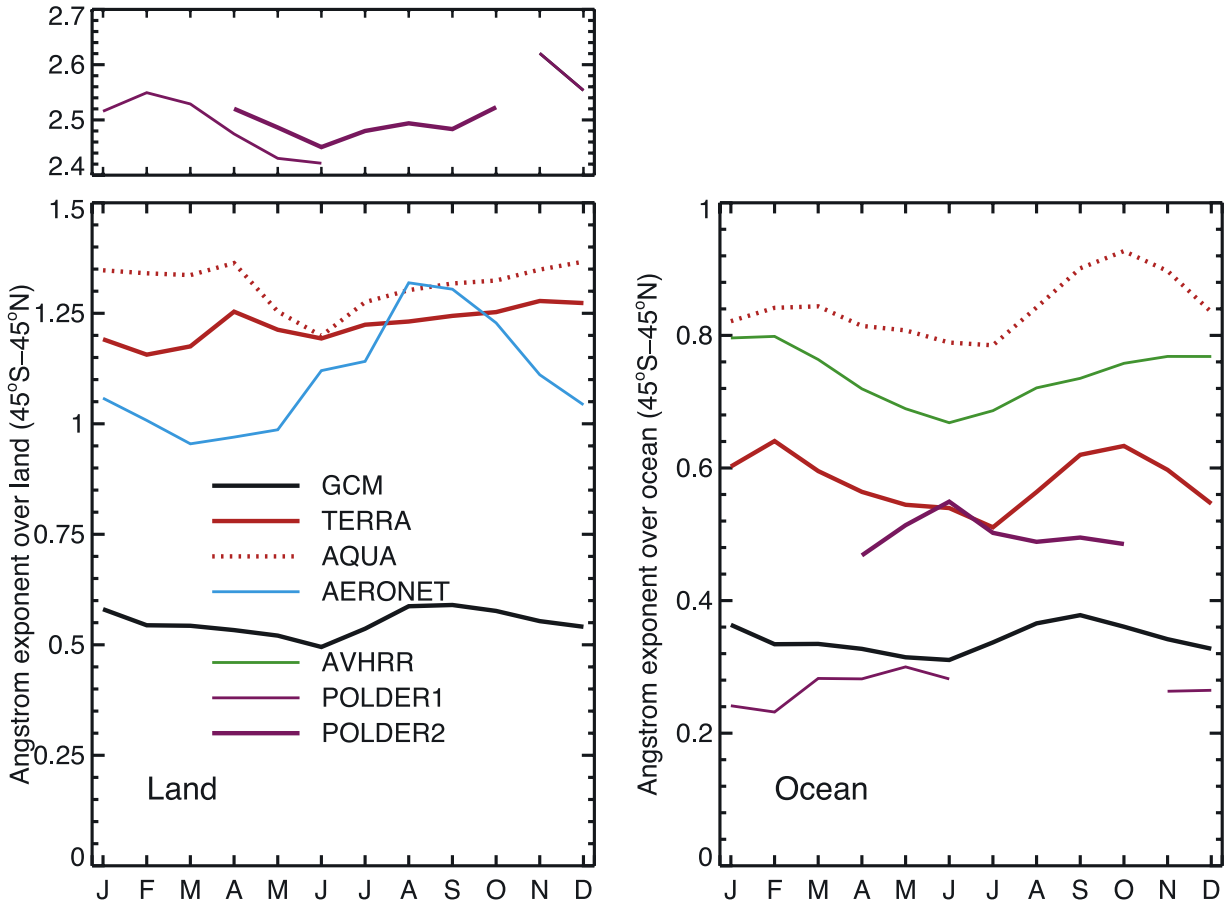

Figure 5. Same as Figure 4 but the averaged data are for the Ångström exponent.

depths at high latitudes, related perhaps to more severe problems with cloud screening, the latitude range in Figures 4 and 5 was constrained to 45°S–45°N. Figure 4 shows that although MODIS and MISR generally tend to agree on the relative shape of the seasonal cycle of aerosol optical depth over both land and ocean, they disagree on the magnitude of the optical depth. Figure 4 (left) shows the MODIS retrieved optical depths over land to be substantially higher than MISR while the reverse is true over ocean (Figure 4, right), as previously noted in the intercomparison study by *Abdou et al.* [2005]. AVHRR retrieved optical depths over ocean, while similar in magnitude to MODIS-Aqua, differ in the shape of the seasonal cycle. POLDER2 derived optical depths tend to agree better with the other data sets than POLDER1 although they both have the same basic instrument design. The differences appear to be the result of POLDER2 utilizing a more realistic bimodal aerosol model comprising a fine and coarse mode, as typically found in AERONET retrievals [*Eck et al.*, 1999; *Dubovik et al.*, 2002], compared to the less realistic monomodal aerosol model used in the POLDER1 retrieval algorithm. AERONET retrievals over land are also different from the satellite based observations, but this could be due to sparse and geographically uneven sampling of AERONET sites. Meanwhile, the seasonal cycle of GCM aerosols is decidedly different from all of the observational data sources over both land and ocean. A closer look finds that such a overall deviation of the seasonal shape from that of the observations mainly originate from tropical aerosols between 20°S–20°N. Further studies are needed before rendering any firm conclusions and a possible improvement.

[20] Differences between the different data sets become more pronounced when the size of the aerosol is considered. The aerosol Ångström parameter has values that range from 0.2 (POLDER1) over the ocean to over 2.5 (POLDER1 and 2) over the land (Figure 5). While the GISS ModelE Ångström exponent is close to POLDER1 results over the ocean, it is well below the lower bound of the observed range for this parameter over land. It is disconcerting that MODIS-Aqua gets a 50% higher Ångström exponent than MODIS-Terra over ocean (Figure 5, right), particularly since MODIS-Terra and MODIS-Aqua utilize the same basic satellite sensors and retrieval algorithms. An obvious difference is their equator crossing time, 1030 LT for Terra and 1330 LT for Aqua, respectively, but it is unlikely that the large difference in Ångström exponent can be attributed to diurnal variations in aerosol size, or to the different viewing geometries, considering MODIS's broad spectral range and use of vector radiative transfer modeling in their retrieval algorithm [*Levy et al.*, 2004]. Such large discrepancy in Ångström exponent between Terra and Aqua may be indicative of differences in calibration and/or retrieval algorithms for

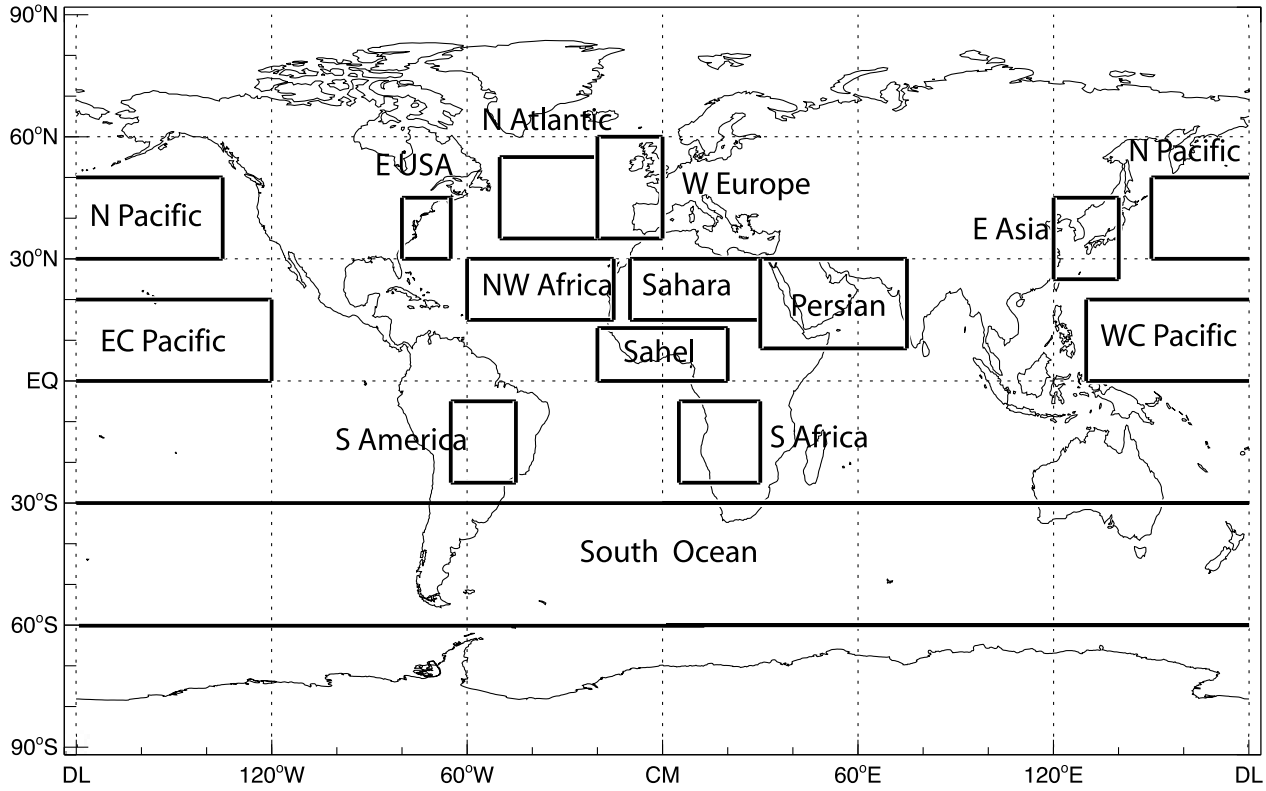

Figure 6. Regions selected for comparisons. For those containing both land and ocean masses, averages are calculated over water and land surfaces separately.

the two data sets. Indeed, January 2004 adjustments to the Terra retrieval algorithm have brought the Ångström Exponent into better agreement with that from Aqua with little impact on the retrieved aerosol optical depth (L. Remer, private communication, 2006). The AVHRR retrieved Ångström exponent is close in magnitude to that of MODIS-Aqua, while POLDER 2 is similar to MODIS-Terra (Figure 5, right). Meanwhile over land (Figure 5, left), the much higher POLDER retrieved Ångström exponents (~2.5) appear to be consistent with the polarization signal that would be expected from accumulation mode aerosols ($r_{\text{eff}} \sim 0.1$ μm) as discussed above.

3.1.2. Regional Scale

[21] To help isolate and localize the spatial and seasonal differences in aerosol variability, and to examine the satellite−model differences in light of different aerosol components, a number of key geographic locations have been marked off as shown in Figure 6. These regions represent major aerosol regimes, e.g., dust pollution in Persian Gulf, from Sahara desert and off the west coast of Africa; biomass burning in South America and Africa; biomass burning combined with the southward flow of mineral dust from the Sahara desert in Sahel [*Prospero et al.*, 2002]; sea salt aerosols in southern oceans and central Pacific; other regions (east United States, west Europe, east Asia, North Atlantic, and North Pacific) are affected by both natural and anthropogenic aerosols components with no single predominant aerosol species. Figure 7 shows the seasonal variability of overall monthly mean aerosol optical depth for the selected regions. The averages are computed separately over water surfaces (top three rows) and land areas (bottom three rows) whenever the specified regions contain both land and ocean scenes, keeping in mind the difficulties of remote sensing of aerosols accurately over the land. The corresponding ModelE aerosol compositions that contribute to the total aerosol optical depth are shown in Figure 8. Though different in magnitude, for the most part, the seasonal profiles of aerosol optical depth for the GCM and the different satellite data sets tend to agree with each other (Figure 7). The seasonality of MODIS-Terra and MODIS-Aqua AOD resembles that of MISR except that the AOD_{MISR} is systematically higher than the $\text{AOD}_{\text{MODIS}}$ over the ocean (top three rows), while the reverse is true over the land (bottom three rows). POLDER2 aerosol optical depth data over the land are biased low, particularly over the regions where coarse particles such as dust and sea salt aerosol dominate (see AOD distributions in Sahara, Persian, and Southern Ocean). There is generally good agreement between $\text{AOD}_{\text{AVHRR}}$ and the AODs derived from other more advanced satellites despite the fact that the AVHRR instrument has only two spectral channels to retrieve aerosol properties.

[22] Specifically, the Persian Gulf area appears to have the closest match between GCM model results and satellite observations, with the same basic seasonal cycle and similar amplitude. The seasonal variation of AOD_{GCM} also agrees with satellite retrievals in west Europe, North Atlantic, and North Pacific except during some winter months (DJF). Cursory inspection of the relative contributions of each principle aerosol component in the ModelE

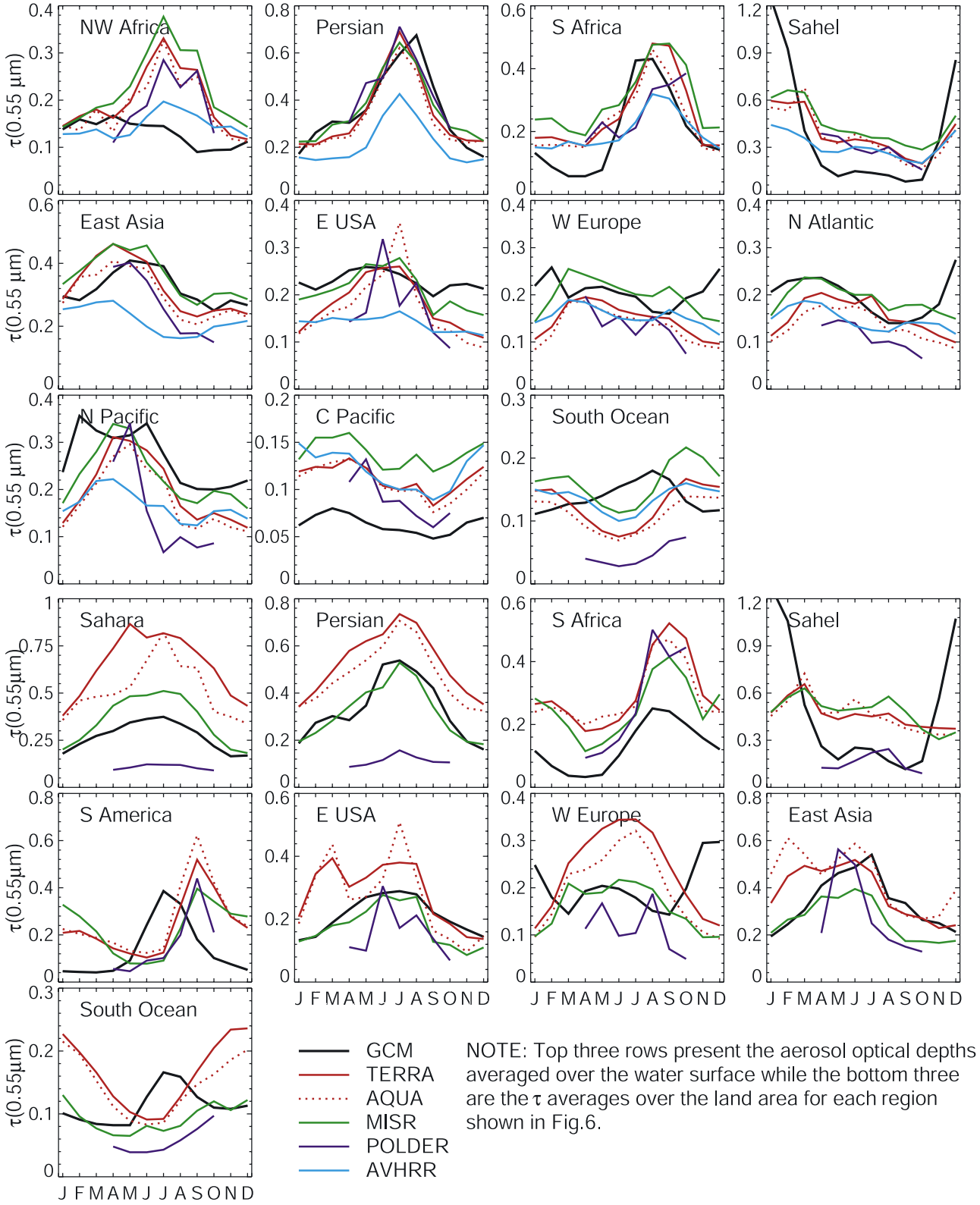

Figure 7. Regional analysis of overall monthly mean aerosol optical depth averaged over the various aerosol regimes shown in Figure 6 as a function of time. Averages are computed only over water surfaces (top three rows) and land areas (bottom three rows) if the designated area contains both land and water masses.

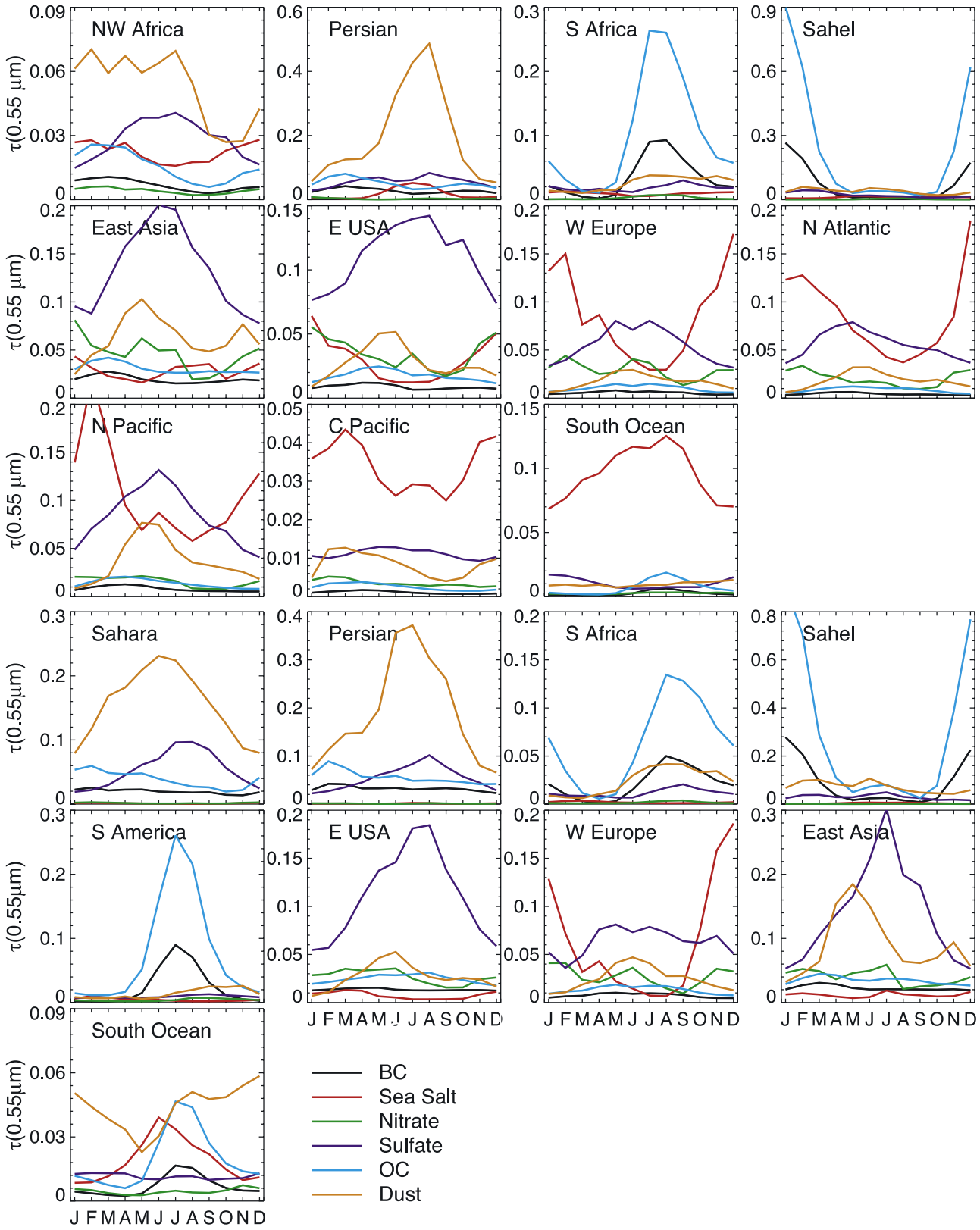

Figure 8. Relative contributions of each principle aerosol component considered in the GCM to the total aerosol optical depth.

climatology (Figure 8) reveals a much higher sea salt concentration during the winter in these three areas, which may well be the cause of the deviation of the overall AOD_{GCM} seasonal shape from satellite measurements.

[23] Over South Africa, the GCM and satellite observed seasonal minima occur at the same time, but the GCM maximum value comes about a month earlier than the satellite retrievals. A possible reason for this phase shift may lie in the modeling of biomass burning aerosols (BC + OC, see Figure 8). Compared with satellite observations, the GCM aerosol optical depth in the Sahel region is far too high during the December–January time period. However, it is possible that satellites may underestimate the true aerosol amount during peak burning seasons by classifying thick smoke as cloud. Likewise in South Africa, the GCM appears to underestimate the background aerosols in the Sahel region during nonburning seasons.

[24] The influence of westward transport of Saharan dust can be clearly seen in northwest Africa where the peak AOD values of MODIS and MISR reach as high as about 0.35 in July, whereas the GCM gets significantly lower optical depths. This may be attributed to weaker sources, and possibly weaker transport and/or strong deposition in the model.

[25] The central Pacific and Southern Ocean regions represent two clean oceanic sites that are dominated by sea salt aerosol (see Figure 8). Over the central Pacific, the GCM aerosol is strongly lower than observations, but with the same general seasonal variability. In contrast, the Southern Ocean region is a problem area where the seasonal cycle of the GCM aerosol is of opposite phase to the observed variability (see Figure 7). The GCM shows the peak optical depth as occurring in August (in agreement with peak wind speeds in the Southern Ocean regions), whereas all of the satellite data (MODIS, MISR, AVHRR, POLDER) have the aerosol optical depth minimum occurring in June to July. Potential cloud contamination is always a problem in this heavily clouded region. Further investigation is needed to explain this perplexing inconsistency between the model derived and the satellite observed results in this area.

[26] Meanwhile, over the land (bottom three rows of Figure 7), the GCM achieves reasonable agreement with MISR, over the Persian Gulf, Sahara Desert, east United States, and east Asia areas. The MODIS optical depth appears to be biased high relative to MISR and POLDER2 over land, and also with respect to AERONET measurements. The seasonal dependence of the different AOD data sets follows the same basic shape as observed over the water surfaces in the same region, and thus will not be discussed specifically.

[27] In contrast to the aerosol optical depth, the Ångström exponent has a less well defined seasonal structure (Figure 9). As in Figure 7, the Ångström exponents are also separately averaged over water surfaces (top three rows) and land areas (bottom three rows). MODIS-Terra and MODIS-Aqua tend to have the same seasonal dependence, but there appears to be a constant bias in that MODIS-Aqua has consistently higher Ångström exponents than MODIS-Terra over ocean. Interestingly, the differences in Ångström exponent between MODIS-Terra and MODIS-Aqua are significantly smaller over the land than over the ocean, even though aerosol retrievals are more robust over ocean because of its near uniform dark surface and a more robust retrieval algorithm. Overall, it is seen that the satellite derived Ångström exponents reach their maximum values in summer presumably because more sulfate aerosols are produced during this season, except in the Persian Gulf where A is minimum during the summer dust outbreak season and in South African and Sahel regions where the maximum A values appear around the biomass burning season. In clean environment such as central Pacific, there is little seasonal variability in Ångström parameter. Perhaps because of the limited spectral information, no clear seasonality can be discerned from the AVHRR Ångström exponent climatology, except in Persian Gulf and Southern Ocean regions.

[28] The seasonal variation of the GCM Ångström exponent over the ocean (top three rows) shows reasonable similarity to the satellite retrievals, given the large uncertainties inherent in the satellite data themselves. However, the magnitude of the GCM Ångström values is systematically biased low compared to the satellite retrievals. This implies that the aerosol effective radii specified in the model are too large (see Figure 3). The Persian Gulf, northwest Africa, east United States, and central Pacific appear to have the closest match in terms of seasonal shape between GCM model results and satellite observations. Over the land surfaces, the GCM Ångström exponent tends to agree with MODIS data in the Sahara and Persian regions, but is biased low in other places with a much smaller seasonal amplitude.

3.1.3. Local Scale: Comparison With AERONET Data

[29] AERONET measurements provide the most localized estimates of aerosol properties with perhaps the best cloud screening capability. In Figure 10, we assume a flat trend for the GCM aerosol beyond 1990 and compare the ModelE aerosol climatology with AERONET measurements, along with other satellite data sets, at five isolated island locations: Amsterdam Island in the Indian Ocean and Midway, Nauru, Lanai, and Tahiti in the Pacific Ocean. On a local scale, the time series of AVHRR retrievals is noisy and often suffers from frequent missing data at certain times and locations because of the limitation of the sparse sampling of the ISCCP DX data [*Rossow and Schiffer*, 1999]. MISR get systematically higher optical depths at all locations except Lanai, consistent with what is observed at larger scales. At the more remote Amsterdam Island, Midway Island, and Nauru, MODIS-Terra and AERONET agree on both the aerosol optical depth and Ångström exponent. MODIS-Aqua is consistently biased higher than Terra for the Ångström exponent at all five locations. At Lanai and Tahiti, the AERONET Ångström exponent is seen to be higher than both Aqua and Terra, but the corresponding AERONET optical depth is decidedly less than either Aqua or Terra. The most likely explanation for these results is that cloud screening is less of a problem at the other sites, but that at Lanai and Tahiti, both Aqua and Terra are significantly impacted by subpixel cloud contamination (thus producing a larger optical depth and a lower Ångström exponent), whereas AERONET, by the nature of its solar beam extinction measurements, is better equipped to screen out small clouds than Aqua or Terra. It is seen that POLDER2 Ångström exponents are closer to MODIS-Terra than to MODIS-Aqua at all locations. Meanwhile, the GCM has good agreement with AERONET data in terms of seasonality and amplitude of aerosol optical depth and Ångström exponent at Amsterdam Island and Midway

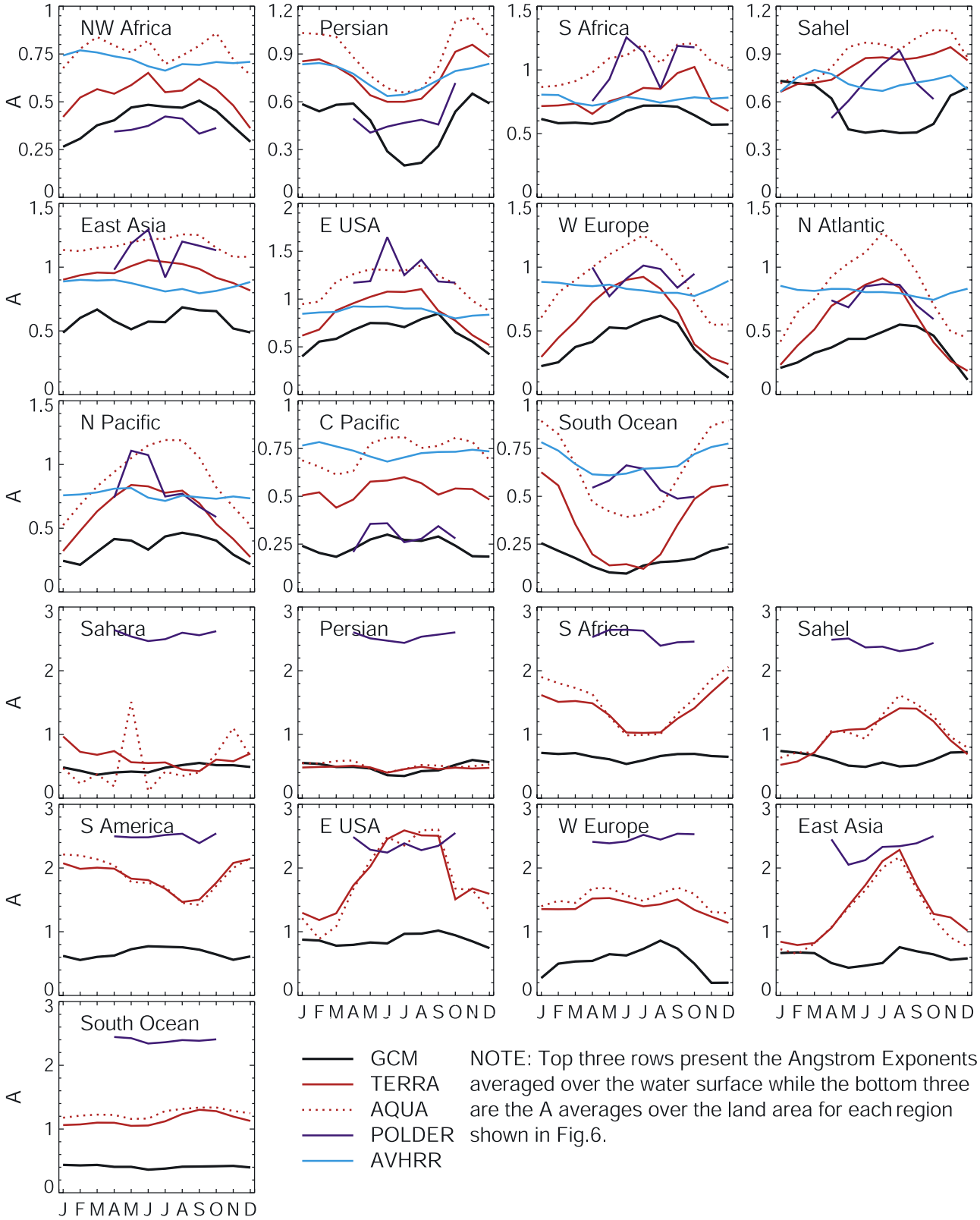

Figure 9. Ångström exponent climatology over the different areas shown in Figure 6. Averages are obtained over water and land surfaces respectively if the designated areas contain both land and ocean masses.

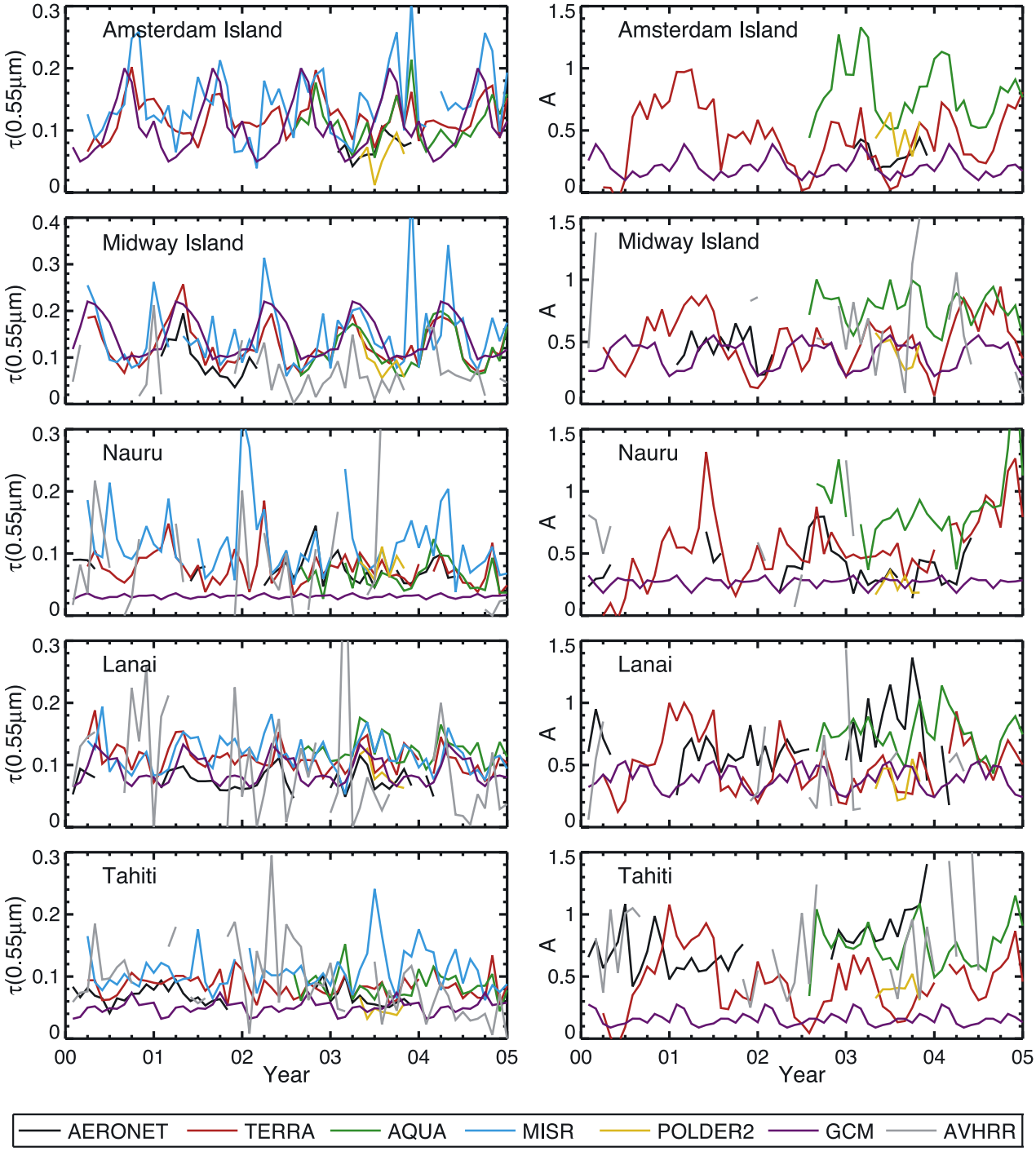

Figure 10. (left) Aerosol optical depth and (right) Ångström exponent monthly mean time series at five isolated sites as measured by AERONET (black curves) and by different satellites. GCM aerosol climatology is also included and depicted by purple curves.

Island. However, at places like Nauru, Lanai, and Tahiti, both AOD and A are underestimated.

3.2. Single Scattering Albedo

[30] The single scattering albedo is the next most important aerosol parameter to be compared against observational data. Ground-based measurements from the AERONET network (more than 390 sites) utilize the direct beam and diffuse radiances [*Dubovik and King*, 2000] to derive the spectral dependence of the column integrated aerosol single scattering albedo. Remote sensing of aerosol single scattering albedo using TOMS data has been discussed by *Torres et al.* [1998]. The results however are strongly dependent on the prescribed surface reflectivity and the assumed height of

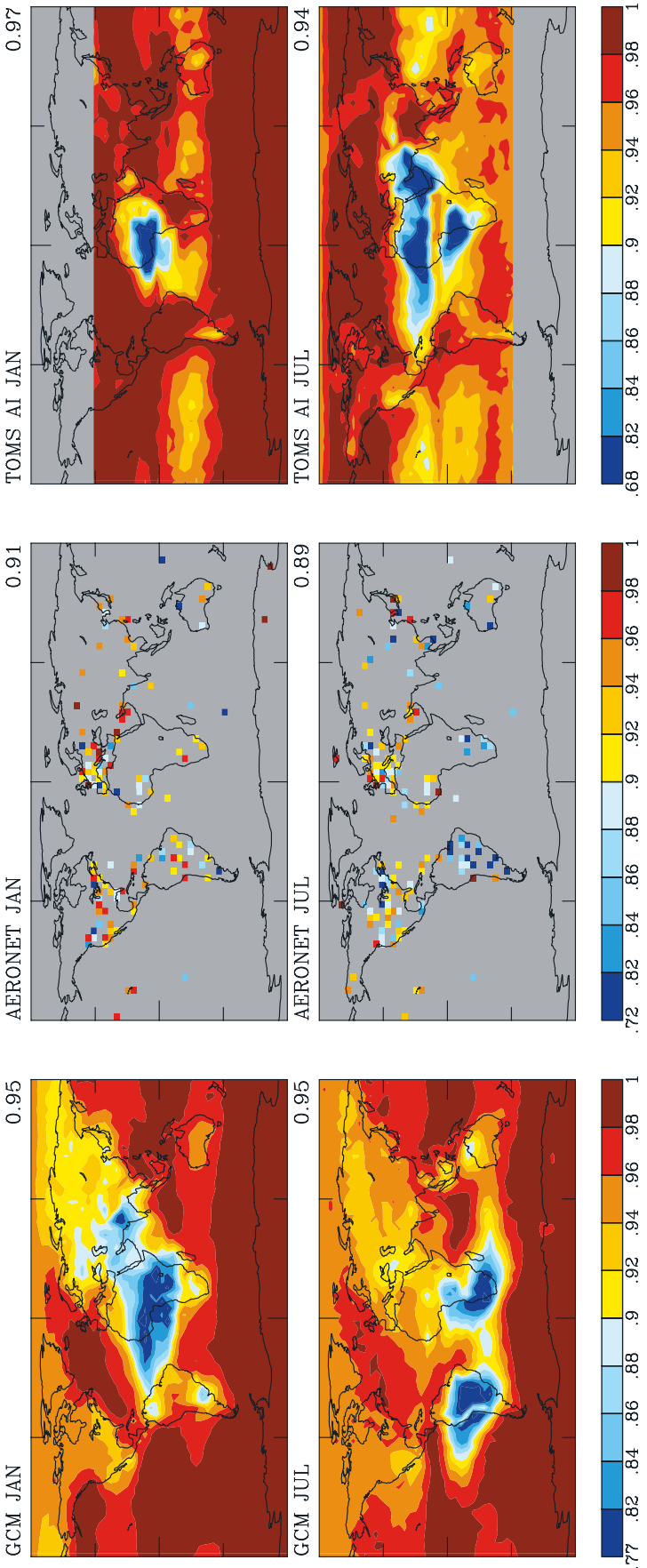

Figure 11. (left) January and July monthly mean single scattering albedo for the GISS ModelE aerosol climatology for 1990. (middle) Aerosol overall monthly mean single scattering albedo measured locally at AERONET network sites. (right) TOMS Aerosol Index (AI) for year 1990, rescaled as $(1-0.1 \times \mathrm{AI})$ to roughly resemble the GCM single scattering albedo. Numbers appearing in the top right corners are area weighted global mean values.

the aerosol layer. They also suffer from subpixel cloud contamination. For example, a 10% subpixel cloud contamination produces an ϖ overestimation of about 0.15, and a ±1 km uncertainty in aerosol height leads to an error in ϖ up to 0.04 [*Torres et al.*, 1998]. Because of these difficulties, the single scattering albedo is not an operational product of TOMS data. Rather, the TOMS Aerosol Index (AI) provides a measure of the spatial and seasonal variability of absorbing aerosols.

[31] Figure 11 shows January and July monthly mean single scattering albedo for the GISS ModelE aerosol climatology for 1990, the corresponding TOMS AI observations, and the overall monthly mean ϖ at 0.44 μm in January and July retrieved from the AERONET measurements. To facilitate comparison with the GCM results, a crude rescaling of the TOMS Aerosol Index by $(1-0.1 \times \mathrm{AI})$ has been included in Figure 11. However, the large differences in the patterns of peak absorptivity suggest that this scaling may be too crude, and that a more detailed simulation of the TOMS AI that explicitly includes the optical depth and height distribution of each GCM aerosol species, is required to achieve a more productive comparison. Nevertheless, as shown in Figure 12, where the difference between GCM and AERONET single scattering albedo is plotted, it is apparent that the GISS GCM overestimates the aerosol single scattering albedo (and thus underestimates the aerosol absorption) at many AERONET locations. However, there is excess GCM absorption at a number of grid boxes spanning northern Africa and the Persian Gulf. Previous comparison of the GISS GCM aerosol with AERONET retrievals by *Sato et al.* [2003] showed a similar difference. On the basis of in situ measurements, satellite retrievals, and modeling studies [*Kaufman et al.*, 2001; *Dubovik et al.*, 2002; *Colarco et al.*, 2002; *Sinyuk et al.*, 2003], the imaginary part of the refractive index of dust aerosols in ModelE [*Patterson et al.*, 1977] was replaced by *Sinyuk et al.* [2003], which put dust absorption in better agreement with AERONET results and TOMS retrievals. With this refractive index change, the global area-weighted annual mean dust single scattering albedo is now 0.965 at 0.55 μm, compared to 0.892 before. Evidently, a local overestimate of black carbon aerosol, given its strong absorption, is a possible explanation since there are still large uncertainties in the modeled BC mass fraction and particle size distributions. On the other hand, uncertainty in the AERONET retrieved single scattering albedo [*Dubovik et al.*, 2000], up to 0.03, also exists.

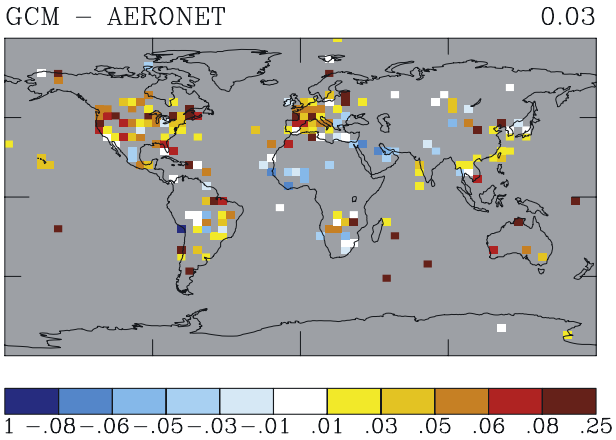

Figure 12. Differences in the GISS GCM and AERONET overall annual mean single scattering albedo. The single scattering albedo is reported at 0.55 μm for the GCM, while the selected AERONET wavelength is 0.44 μm. The number in the top right corner represents area weighted global mean.

4. Discussion

[32] There is a substantial agreement as well as substantial discrepancy between the GCM aerosol optical depth, Ångström exponent, and single scattering albedo climatology and observational data. This can be attributed to many factors such as problems of space-time sampling, differences in microphysical and optical parameters used in the model and in the retrieval algorithm, and errors that originate from the chemical-transport model upon which the GCM aerosol climatology is based. Overall, the intercomparison suggests that the prescribed sizes in the GISS GCM aerosol climatology are too large and should be reduced to obtain a better fit to the observed Ångström exponent (Figures 2, 5, 9, and 10). This reduction in size may in turn increase the aerosol optical depth to be in better agreement with observed results. However, given that there are large differences between measurements, it is problematic to define a "general consensus for ground truth." This also points to a continued need for improvement of the global satellite retrievals of tropospheric aerosols [*Mishchenko et al.*, 2004].

[33] In view of the fact that readjusting GCM aerosol sizes will also impact the aerosol optical depth distributions, and perhaps even change the seasonal cycle, it is logical to first address the Ångström exponent issues. AERONET measurements undoubtedly provide the best observational estimates of aerosol size over land. The AERONET network measures spectral extinction by aerosols from direct beam observations of the sun, including an independent derivation of the Ångström exponent from almucantar measurements of diffuse skylight [*Eck et al.*, 1999]. Both sets of measurements agree well with each other, and also with a series of higher spectral and time resolution measurements made with RSS and MFRSR shadow-band instruments at the ARM SGP site in Oklahoma that included the use of a more robust cloud-screening algorithm [*Alexandrov et al.*, 2005]. As evident from the Ångström exponent dependence on aerosol effective radius in Figure 3, the GCM aerosols over land appear to be larger than 0.3 μm, whereas AERONET suggests a value closer to 0.2 μm. In contrast, satellite retrievals entail more modeling complexities than the AERONET measurement because the satellite spectral radiances must first be converted to aerosol extinction optical depths using tabulated radiative transfer model results, which depend on knowledge of aerosol radiative parameters and properties that are not a priori available to the retrieval. Moreover retrieval of the spectral dependence of aerosol optical depth from which the Ångström exponent is derived is fairly sensitive to nonlinearities in instrument calibration particularly at the low intensity end of the scale [*Remer et al.*, 2005]. Also, screening out subpixel cloud contamination, thin cirrus, and scattered light from nearby

cloud fields is necessarily different for the different instruments and retrieval algorithms, and is unlikely be accomplished with complete success. The MODIS retrieval algorithm over land uses measured reflectances in only three spectral bands, and since the land surface variability can dominate the total signal, hence both AOD and Ångström exponent retrievals are more dependent on model assumptions [*Levy et al.*, 2004]. The MODIS algorithm over ocean is more robust since it makes use of six spectral bands from 0.55 μm to 2.13 μm and utilizes vector radiative transfer to model polarization effects within the atmosphere [*Tanré et al.*, 1997; *Levy et al.*, 2003, 2004; *Remer et al.*, 2005], although apparently the 1.64 μm spectral channel for Aqua is defective, so that only 5 spectral wavelengths are used to derive aerosol properties over ocean from MODIS-Aqua. The AVHRR retrieved Ångström exponent, based on ISCCP DX data, uses only two spectral channels [*Mishchenko et al.*, 2003] and is available only over ocean. POLDER1 has the same basic instrumentation as POLDER 2, but uses a monomodal aerosol model in its retrieval while POLDER2 utilizes a more realistic bimodal aerosol comprising a fine and coarse mode. The previous analysis shows that over the ocean the AVHRR retrieved Ångström exponent is close in magnitude to MODIS-Aqua, while POLDER2 is similar to MODIS-Terra, with POLDER1 getting the smallest A (Figure 5). Meanwhile over land, POLDER appears to be sensitive only to the accumulation mode signal; MODIS-Terra and MODIS-Aqua are close to each other in magnitude, but are systematically higher than the AERONET data. There is no obvious choice for the "consensus ground truth" and no simple explanation for the rather large differences between the different observational results. Nevertheless, on the basis of the good agreement between MODIS-Terra and the second generation polarimetric POLDER2 retrieval results for the Ångström exponent, and the fact that MODIS-Terra is in better agreement with the AERONET measurements (Figure 10), preference should probably go to MODIS-Terra over the MODIS-Aqua and AVHRR combination.

[34] In support of this, it is found that the MODIS-Terra overall fine mode fraction product is closer to AERONET than that of Aqua (L. Remer, private communication, 2005), which reinforces our preference of Terra over Aqua. Accordingly, it seems reasonable to use the AERONET results for Ångström exponent over land, and MODIS-Terra results over ocean for readjusting the GCM aerosol sizes. The caveat remains that cloud contamination may still be an important issue that requires further evaluation.

[35] While there is qualitative agreement between the GCM and satellite observed aerosols in general, of particular concern is the total disagreement in the phase of the seasonal cycle of the aerosol optical depth over the Southern Ocean region (30°S to 60°S, see Figure 7). Without exception, all of the satellite data show the aerosol optical depth to be minimum in June to July. As shown in Figure 8, the GCM composition of the Southern Ocean aerosol is predominantly sea salt. The sea salt aerosol is taken from the chemistry-transport model results of *Chin et al.* [2002], which utilize satellite observed winds from SSM/I [*Atlas et al.*, 1996] and empirical relationships from *Gong et al.* [1997] to compute the sea salt distributions. Because the average lifetime of sea salt particles is very short, there is every reason to expect the sea salt aerosol optical depth to be closely correlated with the local wind speed, whose maximum value occurs during July in the Southern Ocean region. Accordingly, there is strong reason to suspect that the satellite retrievals of aerosol optical depth in the Southern Ocean region are subject to sampling biases and/or cloud contamination that affect the seasonal dependence of the retrieved aerosols, as evidenced in part by the fact that MODIS and ISCCP do not agree on the seasonal variation of cloud fraction in the south ocean region. Remarkably, all the satellite retrievals, MODIS, MISR, POLDER, AVHRR, exhibit the same seasonal retrieval bias. Otherwise there must be something seriously remiss with the chemistry-transport model calculations of sea salt aerosol distribution and seasonal variability.

[36] Despite its climatological importance, current satellite measurements are not sufficient to accurately retrieve the aerosol single scattering albedo. At present, AERONET measurements provide the principle means for validating the GCM single scattering albedo. In the future, Aerosol Polarimetry Sensor (APS), to be launched in 2008, will provide improved measurement of the global distribution of absorbing aerosols.

[37] Overall, the foregoing clearly demonstrates that aerosol sizes are overestimated in the GISS ModelE aerosol climatology. However, since the satellite retrieved aerosol properties are column integrated quantities and do not discriminate aerosol types, improving the size specification in the model is not a simple task. A simple across the board rescaling of the sizes of the different GCM aerosol species may not be sufficient to simultaneously fit both the observed optical depth and Ångström exponent while retaining agreement with the geographical and seasonal variability. How best to resolve these issues and achieve an improved GISS GCM aerosol climatology entails further research efforts.

[38] It should be noted that as satellite retrieval algorithms continue to be upgraded and as GCM modeling results improve, characteristics of the model-satellite data intercomparisons are likely to change. MODIS Collection 005 data are expected to be available by the end of 2006 (L. Remer, e-mail communication, 2006). On the GISS ModelE side, sulfur and sea salt model simulations have been upgraded and improved [*Koch et al.*, 2006], and there is ongoing effort to improve the aerosol modeling to better address the questions of global climate change.

5. Summary

[39] In this study, we have compared the aerosol climatology that is used in the current ModelE version of the GISS GCM using the available satellite data sets and ground measurements. Generally speaking, in regard to the seasonal variability of aerosol optical depth, MISR and MODIS tend to agree with each other, but they disagree with respect to the magnitude of the optical depth. MODIS retrieved optical depths over land are substantially higher than those of MISR while the reverse is true over the ocean. There are appreciable differences in the retrieved Ångström exponent between MODIS-Terra (morning orbit) and MODIS-Aqua (afternoon orbit) over the ocean, with the value of A_{Aqua} significantly

higher that of A_{Terra}. The bias significantly exceeds the daily variability in aerosol size. Although we have tentatively expressed a preference for MODIS-Terra Ångström exponent, the reasons for the large discrepancy are still under investigation. POLDER1 and POLDER2 disagree with each other as well, but these differences are clearly due to the use of a different retrieval algorithm. POLDER2 data appear to be more consistent with the other data sets because the POLDER2 retrieval algorithm uses a more realistic bimodal aerosol model rather than the monomodal size model applied to the POLDER1 data. The POLDER retrieved Ångström exponent over the land is significantly higher than the others because its spectral range is limited to the visible and near infrared. Lacking measurements at longer wavelengths, POLDER instrument cannot successfully detected coarse mode aerosols using polarization measurements, leaving retrieved A biased high. The AVHRR aerosol climatology is close to that of MODIS-Aqua over the ocean. All in all, the large differences between the different data sets indicate a pressing need for a substantial improvement of global satellite retrievals of tropospheric aerosols [*Mishchenko et al.*, 2004]. In particular, there is an urgent need to reexamine the sampling and retrieval methodology of aerosols in high-latitude regions in order to resolve the glaring inconsistency in the seasonal cycle of sea salt aerosol optical depth between satellite retrievals and chemistry-transport model results.

[40] In summary, comparison of the GISS GCM aerosol climatology against available observation data reveals that the GCM aerosol optical depth spatial and seasonal variability shows reasonable agreement with observations, but that the overall magnitude of the AOD is underestimated. The agreement between the GCM Ångström exponent and the satellite data is more or less satisfactory over the ocean, although the values are smaller than observed. Over the land, the GCM Ångström exponent is clearly biased low. These findings point to the need for readjusting the GCM aerosol sizes. Additional indirect evidence comes from model intercomparison studies [*Kinne et al.*, 2003; *Textor et al.*, 2006], which suggested the GISS dry aerosol sizes are larger than those specified in other AEROCOM models. Fixing the aerosol size problem may also increase the aerosol optical depth to be in better agreement with satellite data, which is now underestimated as found in this study and indicated in previous comparisons [*Penner et al.*, 2002; *Kinne et al.*, 2003]. Readjustment of the aerosol sizes may also impact the GCM aerosol single scattering albedo, although this effect is likely to be small. The higher globally averaged GCM single scattering albedo compared to AERONET data implies that a redistribution of the black carbon optical depths in the GCM aerosol climatology may be needed.

[41] **Acknowledgments.** We thank Michael King and Lorraine Remer for their assistance in the processing and interpretation of MODIS-Terra and MODIS-Aqua data and Jack Xiong for clarification of the MODIS instrument calibration issues. We also thank the AERONET team for providing the ground-based Sun photometer aerosol data used in this work. Francois-Marie Bréon is gratefully acknowledged for sharing with us their POLDER data. We thank two anonymous reviewers for many invaluable comments on an earlier version of this paper and Reto Ruedy for help with the ModelE aerosol data. We are grateful to John Martonchik and Dorothy Koch for helpful comments and useful information. This research was supported by the NASA Science Mission Directorate under the EOS RTOP(621-30-89) and by the Office of Science (BER), U.S. Department of Energy, interagency agreement DE-AI02-93ER61744.

References

Abdou, W. A., D. J. Diner, J. V. Martonchik, C. J. Bruegge, R. A. Kahn, B. J. Gaitley, K. A. Crean, L. A. Remer, and B. Holben (2005), Comparison of coincident Multiangle Imaging Spectroradiometer and Moderate Resolution Imaging Spectroradiometer aerosol optical depths over land and ocean scenes containing Aerosol Robotic Network sites, *J. Geophys. Res.*, *110*, D10S07, doi:10.1029/2004JD004693.

Alexandrov, M. D., B. E. Carlson, A. A. Lacis, and B. Cairns (2005), Separation of fine and coarse aerosol modes in MFRSR data sets, *J. Geophys. Res.*, *110*, D13204, doi:10.1029/2004JD005226.

Atlas, R., R. N. Hoffman, S. C. Bloom, J. C. Jusem, and J. Ardizzone (1996), A multiyear global surface wind velocity dataset using SSM/I wind observations, *Bull. Am. Meteorol. Soc.*, *77*, 869–882.

Charlson, R. J., S. E. Schwartz, J. M. Hales, R. D. Cess, J. A. Coakley Jr., J. E. Hansen, and D. J. Hofmann (1992), Climate forcing by anthropogenic aerosols, *Science*, *255*, 423–430.

Chin, M., P. Ginoux, S. Kinne, O. Torres, B. N. Holben, B. N. Duncan, R. V. Martin, J. A. Logan, A. Higurashi, and T. Nakajima (2002), Tropospheric aerosol optical thickness from the GOCART model and comparisons with satellite and sun photometer measurements, *J. Atmos. Sci.*, *59*, 461–483.

Chu, D. A., Y. J. Kaufman, C. Ichoku, L. A. Remer, D. Tanré, and B. N. Holben (2002), Validation of MODIS aerosol optical depth retrieval over land, *Geophys. Res. Lett.*, *29*(12), 8007, doi:10.1029/2001GL013205.

Chylek, P., G. Videen, D. Ngo, R. G. Pinnick, and J. D. Klett (1995), Effect of black carbon on the optical properties and climate forcing of sulfate aerosols, *J. Geophys. Res.*, *100*, 16,325–16,332.

Colarco, P. R., O. B. Toon, O. Torres, and P. J. Rasch (2002), Determining the UV imaginary index of refraction of Saharan dust particles from Total Ozone Mapping Spectrometer data using a three-dimensional model of dust transport, *J. Geophys. Res.*, *107*(D16), 4289, doi:10.1029/2001JD000903.

Deuzé, J. L., P. Goloub, M. Herman, A. Marchand, G. Perry, S. Susana, and D. Tanré (2000), Estimate of the aerosol properties over the ocean with POLDER, *J. Geophys. Res.*, *105*, 15,329–15,346.

Deuzé, J. L., et al. (2001), Remote sensing of aerosols over land surfaces from POLDER/ADEOS-1 polarized measurements, *J. Geophys. Res.*, *106*, 4913–4926.

Dubovik, O., and M. D. King (2000), A flexible inversion algorithm for retrieval of aerosol optical properties from Sun and sky radiance measurements, *J. Geophys. Res.*, *105*, 20,673–20,696.

Dubovik, O., A. Smirnov, B. N. Holben, M. D. King, Y. J. Kaufman, T. F. Eck, and I. Slutsker (2000), Accuracy assessments of aerosol optical properties retrieved from Aerosol Robotic Network (AERONET) Sun and sky radiance measurements, *J. Geophys. Res.*, *105*, 9791–9806.

Dubovik, O., B. Holben, T. F. Eck, A. Smirnov, Y. J. Kaufman, M. D. King, D. Tanré, and I. Slutsker (2002), Variability of absorption and optical properties of key aerosol types observed in worldwide locations, *J. Atmos. Sci.*, *59*, 590–608.

Eck, T. F., B. N. Holben, J. S. Reid, O. Dubovik, A. Smirnov, N. T. O'Neill, I. Slutsker, and S. Kinne (1999), Wavelength dependence of the optical depth of biomass burning, urban, and desert dust aerosols, *J. Geophys. Res.*, *104*, 31,333–31,349.

Geogdzhayev, I. V., M. I. Mishchenko, W. B. Rossow, B. Cairns, and A. A. Lacis (2002), Global two-channel AVHRR retrievals of aerosol properties over the ocean for the period of NOAA-9 observations and preliminary retrievals using NOAA-7 and NOAA-11 data, *J. Atmos. Sci.*, *59*, 262–278.

Gong, S. L., L. A. Barrie, and J.-P. Blanchet (1997), Modeling sea salt aerosols in the atmosphere: 1. Model development, *J. Geophys. Res.*, *102*, 3805–3818.

Hansen, J. E., and L. D. Travis (1974), Light scattering in planetary atmospheres, *Space Sci. Rev.*, *16*, 527–610.

Hansen, J., M. Sato, and R. Ruedy (1997a), Radiative forcings and climate response, *J. Geophys. Res.*, *102*, 6831–6864.

Hansen, J., et al. (1997b), Forcings and chaos in interannual to decadal climate change, *J. Geophys. Res.*, *102*, 25,679–25,720.

Hansen, J., M. Sato, R. Ruedy, A. Lacis, and V. Oinas (2000), Global warming in the twenty-first century: an alternative scenario, *Proc. Natl. Acad. Sci. U. S. A.*, *97*, 9875–9880.

Hansen, J., et al. (2002), Climate forcings in Goddard Institute for Space Studies SI2000 simulations, *J. Geophys. Res.*, *107*(D18), 4347, doi:10.1029/2001JD001143.

Haywood, J., and O. Boucher (2000), Estimates of the direct and indirect radiative forcing due to tropospheric aerosols: A review, *Rev. Geophys.*, *38*, 513–543.

Holben, B. N., et al. (1998), AERONET—A federated instrument network and data archive for aerosol characterization, *Remote Sens. Environ.*, *66*, 1–16.

Ignatov, A., L. Stowe, and R. Singh (1998), Sensitivity study of the Ångström Exponent derived from AVHRR over the oceans, *Adv. Space Res.*, *21*, 439–442.

Intergovernmental Panel on Climate Change (2001), *Climate Change 2001: The Scientific Basis*, edited by J. T. Houghton et al., Cambridge Univ. Press, New York.

Kahn, R., P. Banerjee, and D. McDonald (2001), The sensitivity of multiangle imaging to natural mixtures of aerosols over ocean, *J. Geophys. Res.*, *106*, 18,219–18,238.

Kahn, R., et al. (2005a), MISR calibration and implications for low-light-level aerosol retrieval over dark water, *J. Atmos. Sci.*, *62*, 1032–1052.

Kahn, R. A., B. J. Gaitley, J. V. Martonchik, D. J. Diner, K. A. Crean, and B. Holben (2005b), Multiangle Imaging Spectroradiometer (MISR) global aerosol optical depth validation based on 2 years of coincident Aerosol Robotic Network (AERONET) observations, *J. Geophys. Res.*, *110*, D10S04, doi:10.1029/2004JD004706.

Kaufman, J. Y., D. Tanré, O. Dubovik, A. Karnieli, and L. A. Remer (2001), Absorption of sunlight by dust as inferred from satellite and ground-based remote sensing, *Geophys. Res. Lett.*, *28*, 1479–1482.

Kinne, S., et al. (2003), Monthly averages of aerosol properties: A global comparison among models, satellite data, and AERONET ground data, *J. Geophys. Res.*, *108*(D20), 4634, doi:10.1029/2001JD001253.

Kirchstetter, T. W., T. Novakov, and P. V. Hobbs (2004), Evidence that the spectral dependence of light absorption by aerosols is affected by organic carbon, *J. Geophys. Res.*, *109*, D21208, doi:10.1029/2004JD004999.

Koch, D. (2001), Transport and direct radiative forcing of carbonaceous and sulfate aerosols in the GISS GCM, *J. Geophys. Res.*, *106*, 20,311–20,332.

Koch, D., D. Jacob, I. Tegen, D. Rind, and M. Chin (1999), Tropospheric sulfur simulation and sulfate direct radiative forcing in the Goddard Institute for Space Studies general circulation model, *J. Geophys. Res.*, *104*, 23,799–23,822.

Koch, D., G. A. Schmidt, and C. V. Field (2006), Sulfur, sea salt, and radionuclide aerosols in GISS ModelE, *J. Geophys. Res.*, *111*, D06206, doi:10.1029/2004JD005550.

Lacis, A. A., and M. I. Mishchenko (1995), Climate forcing, climate sensitivity, and climate response: A radiative modeling perspective on atmospheric aerosols, in *Aerosol Forcing of Climate*, edited by R. J. Charlson and J. Heintzenberg, pp. 11–42, John Wiley, Hoboken, N. J.

Lefohn, A. S., J. D. Husar, and R. B. Husar (1999), Estimating historical anthropogenic global sulfur emission patterns for the period 1850–1990, *Atmos. Environ.*, *33*, 3435–3444.

Levy, R. C., L. A. Remer, D. Tanré, Y. J. Kaufman, C. Ichoku, B. N. Holben, J. M. Livingston, P. B. Russell, and H. Maring (2003), Evaluation of the Moderate-Resolution Imaging Spectroradiometer (MODIS) retrievals of dust aerosol over the ocean during PRIDE, *J. Geophys. Res.*, *108*(D19), 8594, doi:10.1029/2002JD002460.

Levy, R. C., L. A. Remer, and Y. J. Kaufman (2004), Effects of neglecting polarization on the MODSI aerosol retrieval over land, *IEEE Trans. Geosci. Remote Sens.*, *42*, 2576–2583.

Liao, H., J. H. Seinfeld, P. J. Adams, and L. J. Mickley (2004), Global radiative forcing of coupled tropospheric ozone and aerosols in a unified general circulation model, *J. Geophys. Res.*, *109*, D16207, doi:10.1029/2003JD004456.

Liousse, C., J. E. Penner, C. Chuang, J. J. Walton, H. Eddleman, and H. Cachier (1996), A global three-dimensional model study of carbonaceous aerosols, *J. Geophys. Res.*, *101*, 19,411–19,432.

Liu, L., M. I. Mishchenko, I. Geogdzhayev, A. Smirnov, S. M. Sakerin, D. M. Kabanov, and O. A. Ershov (2004), Global validation of two-channel AVHRR aerosol optical thickness retrievals over the oceans, *J. Quant. Spectrosc. Radiat. Transfer*, *88*, 97–109.

Martonchik, J. V., D. J. Diner, R. A. Kahn, T. P. Ackerman, M. M. Verstraete, B. Pinty, and H. R. Gordon (1998), Techniques for the retrieval of aerosol properties over land and ocean using multiangle imaging, *IEEE Trans. Geosci. Remote Sens.*, *36*, 1212–1227.

Menon, S., J. Hansen, L. Nazarenko, and Y. Luo (2002), Climate effects of black carbon aerosols in China and India, *Science*, *297*, 2250–2253.

Mishchenko, M. I., I. V. Geogdzhayev, B. Cairns, W. B. Rossow, and A. A. Lacis (1999), Aerosol retrievals over the ocean by use of channels 1 and 2 AVHRR data: Sensitivity analysis and preliminary results, *Appl. Opt.*, *38*, 7325–7341.

Mishchenko, M. I., I. V. Geogdzhayev, L. Liu, J. A. Ogren, A. A. Lacis, W. B. Rossow, J. W. Hovenier, H. Volten, and O. Muñoz (2003), Aerosol retrievals from AVHRR radiances: Effects of particle nonsphericity and absorption and an updated long-term global climatology of aerosol properties, *J. Quant. Spectrosc. Radiat. Transfer*, *79–80*, 953–972.

Mishchenko, M. I., B. Cairns, J. E. Hansen, L. D. Travis, R. Burg, Y. J. Kaufman, J. V. Martins, and E. P. Shettle (2004), Monitoring of aerosol forcing of climate from space: Analysis of measurement requirements, *J. Quant. Spectrosc. Radiat. Transfer*, *88*, 149–161.

Nilsson, B. (1979), Meteorological influence on aerosol extinction in the 0.2–40 μm wavelength range, *Appl. Opt.*, *18*, 3457–3473.

Novakov, T., V. Ramanathan, J. E. Hansen, T. W. Kirchstetter, M. Sato, J. E. Sinton, and J. A. Sathaye (2003), Large historical changes of fossil-fuel black carbon aerosols, *Geophys. Res. Lett.*, *30*(6), 1324, doi:10.1029/2002GL016345.

Palmer, K. F., and D. Williams (1974), Optical properties of water in the near infrared, *J. Opt. Soc. Am. A*, *64*, 1107–1110.

Palmer, K. F., and D. Williams (1975), Optical constants of sulfuric acid: Application to the clouds of Venus?, *Appl. Opt.*, *14*, 208–219.

Patterson, E. M., D. A. Gillete, and B. H. Stockton (1977), Complex index of refraction between 300 and 700 nm for Saharan aerosols, *J. Geophys. Res.*, *82*, 3153–3160.

Penner, J. E., et al. (2002), A comparison of model- and satellite-derived aerosol optical depth and reflectivity, *J. Atmos. Sci.*, *59*, 441–460.

Prospero, J. M., P. Ginoux, O. Torres, S. E. Nicholson, and T. E. Gill (2002), Environmental characterization of global sources of atmospheric soil dust identified with the Nimbus 7 Total Ozone Mapping Spectrometer (TOMS) absorbing aerosol product, *Rev. Geophys.*, *40*(1), 1002, doi:10.1029/2000RG000095.

Remer, L. A., et al. (2002), Validation of MODIS aerosol retrieval over ocean, *Geophys. Res. Lett.*, *29*(12), 8008, doi:10.1029/2001GL013204.

Remer, L. A., et al. (2005), The MODIS aerosol algorithm, products, and validation, *J. Atmos. Sci.*, *62*, 947–973.

Rossow, W. B., and R. A. Schiffer (1999), Advances in understanding clouds from ISCCP, *Bull. Am. Meteorol. Soc.*, *80*, 2261–2287.

Sato, M., J. E. Hansen, M. P. McCormick, and J. B. Pollack (1993), Stratospheric aerosol optical depths, 1850–1990, *J. Geophys. Res.*, *98*, 22,987–22,994.

Sato, M., J. Hansen, D. Koch, A. Lacis, R. Ruedy, O. Dubovik, B. Holben, M. Chin, and T. Novakov (2003), Global atmospheric black carbon inferred from AERONET, *Proc. Natl. Acad. Sci. U. S. A.*, *100*, 6319–6324, doi:10.1073/pnas.0731897100.

Schmidt, G. A., et al. (2006), Present-day atmospheric simulations using GISS ModelE: Comparison to in-situ, satellite and reanalysis data, *J. Clim.*, *19*, 153–192, doi:10.1175/JCLI3612.1.

Sinyuk, A., O. Torres, and O. Dubovik (2003), Combined use of satellite and surface observations to infer the imaginary part of refractive index of Saharan dust, *Geophys. Res. Lett.*, *30*(2), 1081, doi:10.1029/2002GL016189.

Stier, P., et al. (2005), The aerosol-climate model ECHAM5-HAM, *Atmos. Chem. Phys.*, *5*, 1125–1156.

Stowe, L. L., A. M. Ignatov, and R. R. Singh (1997), Development, validation, and potential enhancements to the second generation operation aerosol product at the National Environmental Satellite, Data, and Information Service of the National Oceanic and Atmospheric Administration, *J. Geophys. Res.*, *102*, 16,923–16,934.

Takemura, T., T. Nakajima, A. Higurashi, S. Ohta, and N. Sugimoto (2003), Aerosol distributions and radiative forcing over the Asian Pacific region simulated by Spectral Radiation-Transport Model for Aerosol Species (SPRINTARS), *J. Geophys. Res.*, *108*(D23), 8659, doi:10.1029/2002JD003210.

Tang, I. N. (1996), Chemical and size effects of hygroscopic aerosols on light scattering coefficients, *J. Geophys. Res.*, *101*, 19,245–19,250.

Tang, I. N., and H. R. Munkelwitz (1991), Simultaneous determination of refractive index and density of an evaporating aqueous solution droplet, *Aerosol Sci. Technol.*, *15*, 201–207.

Tang, I. N., and H. R. Munkelwitz (1994), Water activities, densities, and refractive indices of aqueous sulfates and sodium nitrate droplets of atmospheric importance, *J. Geophys. Res.*, *99*, 18,801–18,808.

Tanré, D., Y. J. Kaufman, M. Herman, and S. Mattoo (1997), Remote sensing of aerosol properties over oceans using the MODIS/EOS spectral radiances, *J. Geophys. Res.*, *102*, 16,971–16,988.

Tegen, I., P. Hollrig, M. Chin, I. Fung, D. Jacob, and J. Penner (1997), Contribution of different aerosol species to the global aerosol extinction optical thickness: Estimates from model results, *J. Geophys. Res.*, *102*, 23,895–23,915.

Tegen, I., D. Koch, A. A. Lacis, and M. Sato (2000), Trends in tropospheric aerosol loads and corresponding impact on direct radiative forcing between 1950 and 1990: A model study, *J. Geophys. Res.*, *105*, 26,971–26,989.

Textor, C., et al. (2006), Analysis and quantification of the diversities of aerosol life cycles within AeroCom, *Atmos. Chem. Phys.*, *6*, 1777–1813.

Toon, O. B., J. B. Pollack, and B. N. Khare (1976), The optical constants of several atmospheric aerosol species: Ammonium sulfate,

aluminum oxide, and sodium chloride, *J. Geophys. Res.*, *81*, 5733–5748.

Torres, O., P. K. Bhartia, J. R. Herman, Z. Ahmad, and J. Gleason (1998), Derivation of aerosol properties from satellite measurements of backscattered ultraviolet radiation: Theoretical basis, *J. Geophys. Res.*, *103*, 17,099–17,110.

Volz, F. E. (1973), Infrared optical constants of ammonium sulfate, Sahara dust, volcanic pumice, and flyash, *Appl. Opt.*, *12*, 564–568.

Xiong, X., N. Che, and W. Barnes (2005), Terra MODIS on-orbit spatial characterization and performance, *IEEE Trans. Geosci. Remote Sens.*, *43*, 355–365.

Yu, H., et al. (2006), A review of measurement-based assessments of the aerosol direct radiative effect and forcing, *Atmos. Chem. Phys.*, *6*, 613–666.

B. Cairns, B. E. Carlson, A. A. Lacis, L. Liu, and M. I. Mishchenko, NASA Goddard Institute for Space Studies, 2880 Broadway, New York, NY 10025, USA. (lliu@giss.nasa.gov)